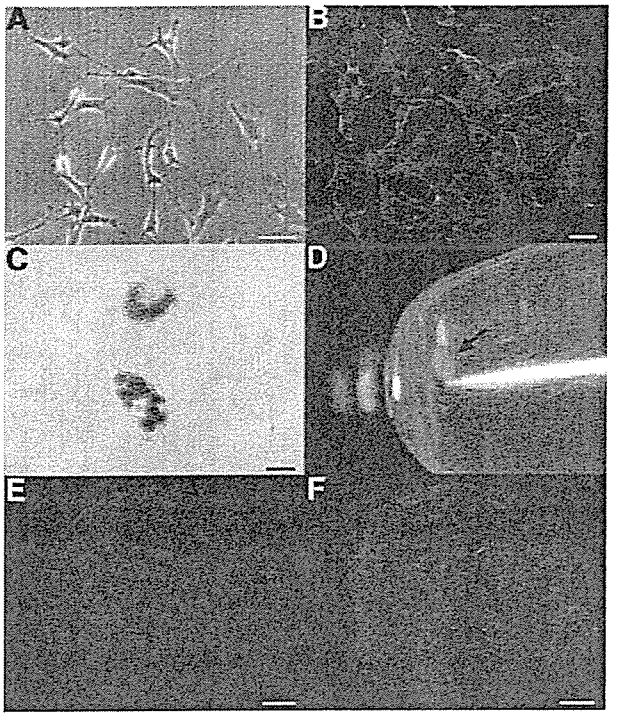

Figure 2. Cornea-derived precursors differentiate into mesenchymal cells. **(A):** Keratocyte phenotype in serum-free culture. **(B):** Anti-α-smooth muscle actin staining of myofibroblasts induced by transforming growth factor (TGF)-β. **(C):** Adipogenic cells stained with oil red O. Cells cultured in medium containing TGF-β3 formed chondrogenic pellets **(D)** (arrow) expressing collagen II **(E)** and aggrecan **(F)**. Scale bars = 50 μm **(A)**, 20 μm **(B, C)**, and 100 μm **(E, F)**.

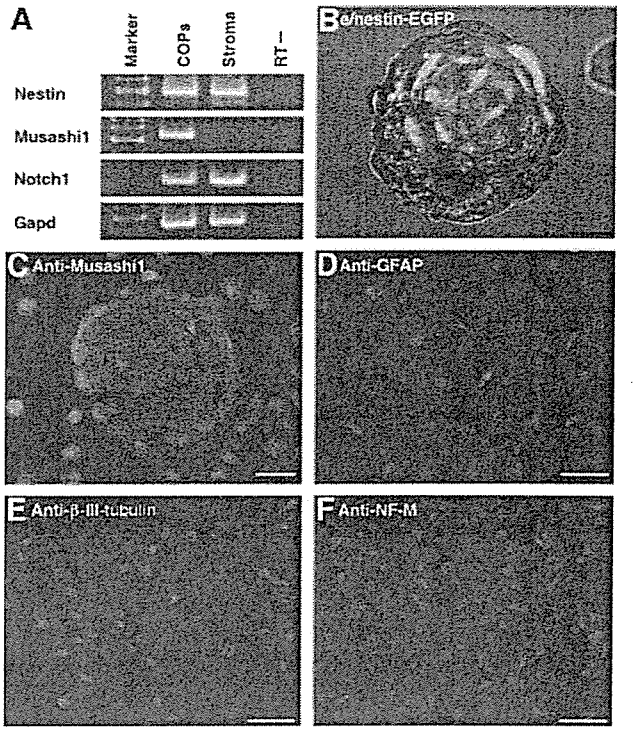

Figure 3. COP spheres express neural stem/precursor and differentiation markers. **(A):** Reverse transcription-polymerase chain reaction analysis of neural stem cell markers *Notch1*, *Musashi1*, and *nestin* expressed in COPs. *Gapd* was loaded as an internal control. **(B):** Fluorescent image merged with transmitted-light image of a COP sphere prepared from an E/nestin-EGFP mouse. EGFP expression confirms the activation of neuronal nestin. **(C):** Immunocytochemical analysis showed high levels of Musashi-1 expressed in COP spheres. Differentiated cells from COP spheres express the neuronal markers GFAP **(D)**, class III-β-tubulin **(E)**, and NF-M **(F)**. Cells were counterstained with 4,6-diamidino-2-phenylindole (blue) to show nuclei. Scale bars = 20 μm **(B, C)** and 50 μm **(D–F)**. Abbreviations: COP, cornea-derived precursor; EGFP, enhanced green fluorescent protein; GFAP, glial fibrillary acidic protein; NF-M, neurofilament-M; RT, reverse transcription.

COPs Differentiate into Neural and Mesenchymal Lineage Cells

COPs differentiate into keratocytes when cultured on plastic (Fig. 2A), into fibroblasts when cultured with serum, and into myofibroblasts under TGF-β stimulation (Fig. 2B) [9]. To determine whether these cells possess the ability to differentiate into other cells of mesenchymal lineage, COPs were cultured in various differentiation-inducing media. After 10 days of culture in medium containing insulin, approximately 7.9% (mean, n = 2) of the cells differentiated into oil red O-positive lipid-producing adipocytes (Fig. 2C). In addition, cell pellets were formed when cells were cultured in chondrogenic-inducing medium containing TGF-β3 (n = 9) (Fig. 2D). Immunofluorescent staining showed expression of the chondrocyte markers, type II collagen and aggrecan [28] in the pellets (Fig. 2E, 2F).

The NSC marker *Msi1*, an RNA-binding protein involved in the maintenance of NSCs and activation of Notch signaling [26, 29, 30], was expressed in COP spheres (Fig. 3A, 3C). COP spheres also expressed the NSC markers *nestin* [25, 31] and *Notch1* (Fig. 3A); the latter is a gene involved in the self-renewal of various types of tissue stem cells, including NSCs [32]. Because Nestin is an intermediate filament expressed by several cell types [33], COP spheres were prepared from E/nestin-EGFP transgenic mice, which carry the EGFP transgene under the control of a NSC-selective enhancer [25]. As expected, EGFP-positive spheres were formed (Fig. 3B) from these mice, which originally did not show EGFP-related fluorescence in the cornea.

Neural differentiation of COPs was shown by the expression of class III β-tubulin, GFAP, and NF-M in cells cultured on poly(L-ornithine)-coated slides in differentiation-inducing medium (Fig. 3E, 3F). Approximately 1.4% of cells stained with anti-NF-M antibody (n = 3), 36.9% $\pm$ 17.7% expressed GFAP (n = 3), and 32.8% $\pm$ 15.8% expressed β-III-tubulin (n = 3).

COP Spheres Are Rich in SP Cells

Several studies have shown that the ability to exclude Hoechst dye is a property of stem cells commonly referred to as SP cells [34], which are distinguished from the "main population" by flow cytometric analysis. The SP cell phenotype is defined by the dye exclusion ability of an ABC transporter, ABCG2, which is inhibited by ABC-transporter inhibitors such as reserpine. We found that COP spheres expressed ABCG2 when examined by reverse transcription (RT)-PCR and immunocytochemistry (Fig.

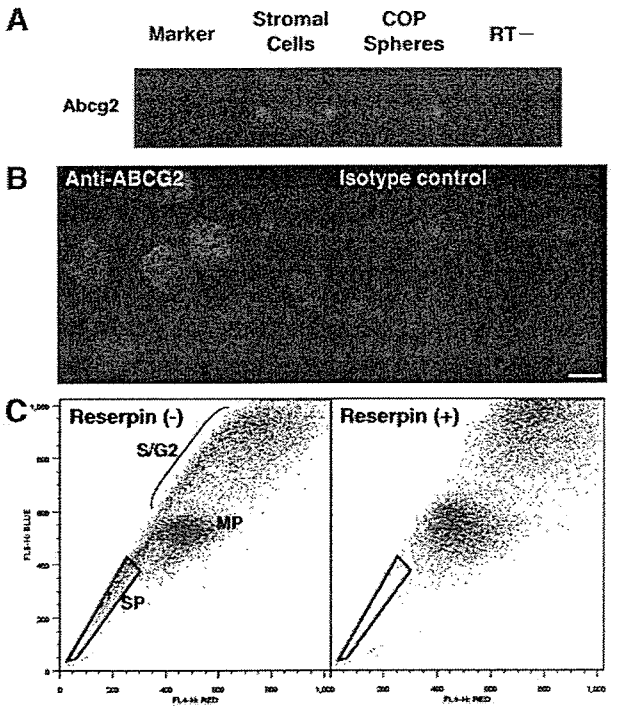

Figure 4. Murine COPs show ABCG2 expression and the SP cell phenotype. **(A):** RT-polymerase chain reaction analysis revealed *Abcg2* expression in COP spheres and in cells freshly dissociated from mouse corneal stroma. **(B):** Immunofluorescent staining of ABCG2 in COP spheres. Nuclei were counterstained with 4,6-diamidino-2-phenylindole. Scale bar = 100 μm. **(C):** Approximately 3.3% of sphere cells were SP cells as shown by flow cytometry. Hypofluorescent SP cells are distinct from MP cells and disappear when treated with reserpine, an inhibitor of ABCG2. Cells in the S/G_2 phase were not gated as SP cells, even though they disappeared with reserpine treatment. Abbreviations: COP, cornea-derived precursor; MP, main population; RT, reverse transcription; SP, side population.

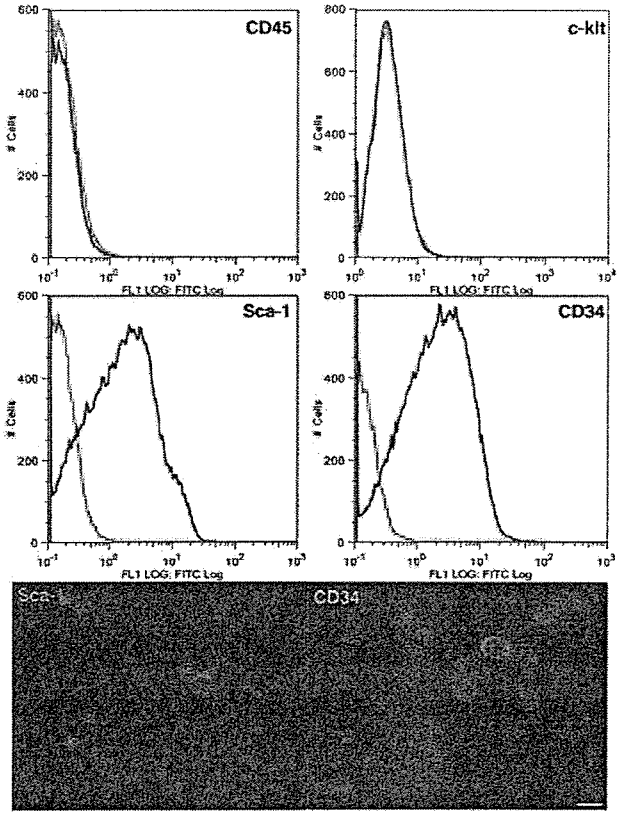

Figure 5. Cornea-derived precursors (COPs) express stem cell surface markers. **(A):** Single cells dissociated from COP spheres were stained with antibodies for CD45, c-kit, Sca-1, or CD34 and analyzed by flow cytometry (blue lines). Red lines represent isotype-matched negative control. COP sphere cells did not express CD45 or c-kit but did express Sca-1 and CD34. **(B):** Fluorescent images of cells stained with phycoerythrin-labeled anti-Sca-1 (left, red) or FITC-labeled anti-CD34 (right, green). Scale bar = 20 μm. Abbreviation: FITC, fluorescein isothiocyanate.

4A, 4B). Reserpine-sensitive SP cells were detected in dissociated sphere cells, representing 3.3% ± 1.2% (n = 8) of viable cells analyzed by flow cytometry (Fig. 4C).

We also analyzed several stem cell-related surface markers by flow cytometry. COP spheres expressed CD34 (Fig. 5A, 5B), a cell surface marker reported in rodent epithelial stem cells in the bulge area [35, 36], skeletal muscle stem cells [37, 38], and corneal stromal cells [9, 39]. In addition, expression of stem cell antigen-1 (Sca-1), a cell surface protein expressed in BM-derived hematopoietic stem cells (BM-HSCs) [40], mammary epithelial stem cells [41], a subpopulation of BM stromal cells [42], skeletal muscle stem cells [38], and SKP spheres [12], was found in 56.1% ± 19.2% (n = 7) of viable cells (Fig. 5). The expression of CD133, found in different types of primitive cells such as BM-HSCs, NSCs, and SKPs [43–46], was not observed (data not shown). Another cell surface marker, c-kit (CD117), the receptor for stem cell factor and a marker of BM-HSCs [47], was also not detected by flow cytometric analysis (Fig. 5) and RT-PCR (not shown).

COPs Are Neural Crest Lineage Cells

Although we found $CD34^+$ cells in COP spheres, Sosnova et al. [48] reported that all $CD34^+$ cells in mouse corneal stroma are $CD45^+$ BM-derived cells. In addition, the ability of BM-derived mesenchymal stem cells (BM-MSCs) to differentiate into multiple cell types has been reported [49, 50]. However, we found that COPs did not express CD45 (0.2% ± 0.2%, n = 6; Fig. 5A), indicating a nonhematopoietic origin for these cells. We further prepared COPs from mice transplanted with GFP^+ WBM cells. GFP^+ cells were not found in COP spheres prepared from the recipient mice 8 weeks after transplantation (Fig. 6C), although numerous GFP^+ cells were observed in the recipient cornea (Fig. 6A, 6B). GFP^+ cells in sphere culture preparations were found attached to the bottom of the culture dish, and immunofluorescent staining showed that the GFP^+ cells were $CD45^+$ and some also expressed CD34 (Fig. 6D). CD34 was therefore expressed in both BM-derived GFP^+ cells as well as GFP-COPs, indicating that WBM-derived cells are not likely to contribute to COP sphere-initiating cells.

Given that cranial neural crest-derived mesenchymal cells contribute to corneal stroma development, we next investigated whether COPs were of neural crest origin [6, 7]. COP spheres were prepared from Wnt1-Cre/Floxed-EGFP and P0-Cre/Floxed-EGFP transgenic mice in which neural crest-derived cells are tagged by EGFP expression [14, 51]. As expected, COP spheres prepared

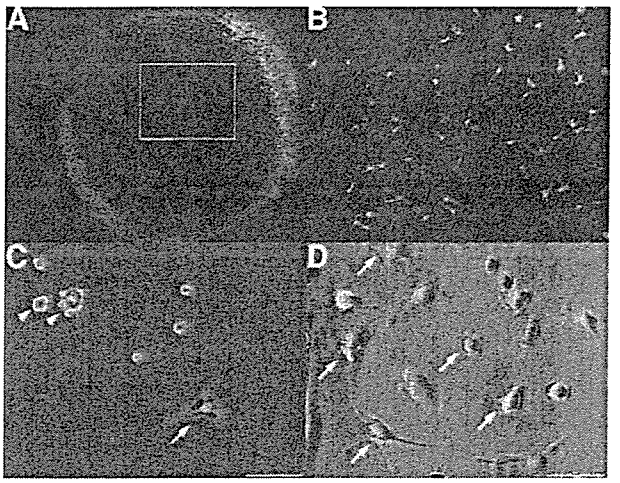

Figure 6. Bone marrow cells do not form cornea-derived precursor (COP) spheres. Sphere cultures prepared from C57BL6/J mice transplanted with whole bone marrow (WBM) cells of green fluorescent protein (GFP) mice did not produce GFP^+ spheres. **(A):** Fluorescent image of a cornea 8 weeks after WBM cell transplantation. Migration of numerous GFP^+ cells into the cornea was observed. **(B):** High-magnification view of the boxed area in (A). **(C):** Phase-contrast image merged with fluorescent image of sphere culture at 7 days after plating. GFP^+ WBM-derived cells were found attached to the culture dish (arrow), whereas GFP^+ cells were not observed in forming spheres (arrowhead). **(D):** Adherent cells were stained with phycoerythrin-labeled anti-CD34 antibody (red). CD34 (arrows) was also expressed in transplanted WBM-derived cells (green). Scale bars = 200 μm **(C, D)**.

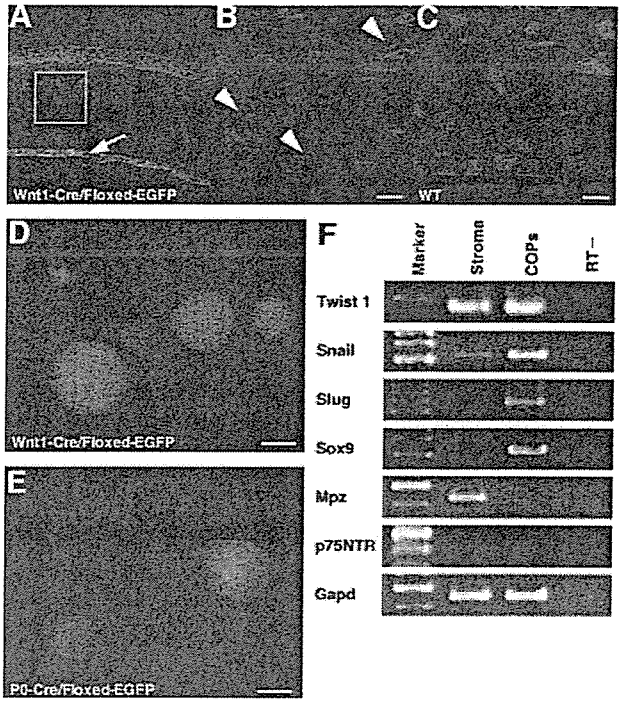

Figure 7. COPs are neural crest-derived cells. **(A–C):** Confocal images of Wnt1-Cre/Floxed-EGFP mouse **(A, B)** and WT mouse cornea **(C)** stained with anti-GFP antibody and cyanine 3-conjugated secondary antibody. **(B):** High-magnification view of the boxed region in (A). Expression of EGFP is detected in keratocytes, although the expression level is low in vivo **(B)** (arrowheads). Positive staining is also detected in corneal endothelium, which is also neural crest-derived **(A)** (arrow). Cells dissociated from corneal stroma of Wnt1-Cre/Floxed-EGFP **(D)** (day 14) and P0-Cre/Floxed-EGFP mice **(E)** (day 6) formed $EGFP^+$ COP spheres. **(F):** Expression of embryonic neural crest markers by COPs and corneal stromal tissue. *Gapd* was loaded as an internal control. Expression of *Snail*, *Slug*, and *Sox9* was upregulated in COP spheres, whereas *Twist* was found in both COPs and stroma. *Mpz* was detected from stromal tissue only. Scale bars = 50 μm **(A, D, E)** and 20 μm **(B, C)**. Abbreviations: COP, cornea-derived precursor; EGFP, enhanced green fluorescent protein; GFP, green fluorescent protein; RT, reverse transcription; WT, wild-type.

from both transgenic mice were GFP^+ (Fig. 7D, 7E). To visualize GFP^+ neural crest-derived cells in the cornea, sections of Wnt1-Cre/Floxed-EGFP mouse were immunostained using anti-GFP antibody. Expression of GFP was detected in stromal keratocytes, although the expression level was low in vivo (Fig. 7B). Strong immunoreactivity was detected in the corneal endothelium (Fig. 7A), which are also neural crest-derived [52, 53]. We also examined embryonic neural crest-associated genes by RT-PCR analysis. *Twist*, *Slug*, *Snail*, and *Sox9* were expressed in COPs (Fig. 7F). These data confirm that COPs are neural crest-derived stem cells that are not recruited from the BM.

DISCUSSION

The expansion of stem cells in vitro while maintaining properties of progenitor cells is critical from the standpoint of using stem cells for research as well as medical purposes. Culture conditions for several adult somatic stem cells, including BM-HSCs and NSCs, have been well-established. The sphere culture technique, which was originally developed for culturing NSCs as neurosphere from the central nervous system (CNS), was recently applied to isolate sphere-initiating cells from adult tissues other than CNS [2, 10–12, 17, 51, 54]. COPs have been subcultured for more than 13 months (more than 18 passages, corresponding to more than 90 population doublings) to date. As we discovered, not only do these cells have the ability to differentiate into keratocytes, fibroblasts, and myofibroblasts as observed in primary stromal keratocytes [9], COPs can also be induced to differentiate into adipocytes, chondrocytes, and neural cells.

Clonal spheres in this study were initiated using methylcellulose, which is an established method to clone hematopoietic cells and, more recently, embryonic stem cells and NCSs [17–24]. Cells within a sphere arising from a single cell were not necessarily homogeneous, which may be due to the position within a sphere or to autocrine and paracrine mechanisms. Dark cells in spheres (Fig. 1) were not GFP-negative but simply had low fluorescence under the conditions of our photography, which were set with exposure settings that do not cause saturation of fluorescent levels. This is vital because long exposure times can give the misleading impression of strong fluorescence in 100% of the cells, which is not the case.

We have also demonstrated that COPs include a high ratio of SP cells with Hoechst dye exclusion activity, which are regarded as a general property of progenitor-candidate cells. Although a higher percentage of cells seem to be ABCG2-positive by immunocytochemical analysis compared with flow cytometry, not all ABCG2-positive cells are drawn into the SP gate, which was defined by the inhibition of functional ABC transporters. Indeed, reserpine-sensi-

tive SP-like cells were found outside the SP gate, which may have been dividing cells exhibiting higher fluorescent intensity. The results of ABCG2 expression in COPs and the high fraction of SP cells suggest that the Hoechst dye exclusion assay may be used to further characterize COPs. A recent study by Du et al. also demonstrated the presence of SP cells in the human peripheral corneal stroma, which were shown to express neural and cartilage markers in addition to keratocyte markers [55]. We have confirmed that COP SP cells re-formed spheres after cell sorting (data not shown).

Other stem cell-related markers, including *nestin*, *Notch1*, and *Msi1*, were also expressed in COP spheres. Although the upregulation of Nestin is often used as evidence of a NSC phenotype, expression of this intermediate filament protein in non-neuronal cells has also been reported [56]. We therefore prepared COP spheres from transgenic mice carrying EGFP under the control of a neural-selective enhancer of the *nestin* gene [57–59]. Given that no fluorescence was observed in corneas of these mice, expression of nestin in corneal stromal cells revealed by RT-PCR analysis is probably due to non-neuronal expression. However, the fluorescence observed in COPs prepared from E/nestin-EGFP transgenic mice suggests that the neural stem/progenitor cell-specific enhancer was activated. Interestingly, we also found that expression of *Msi1* was upregulated only in COPs but not in the corneal stroma of the original mice. Recent reports demonstrated that Msi1 is expressed by epithelial stem cells in intestine [60, 61] and mammary gland [62], making Msi1 a candidate marker of adult stem cells in a variety of tissue sources.

There are only a limited number of reports describing putative progenitor cells for corneal keratocytes [2, 3]. Stromal keratocytes develop from mesenchymal cells originating in the cranial neural crest [6, 7]. A recent study demonstrated that late embryonic keratocytes maintain plasticity to differentiate into other neural crest-derived tissue when transplanted into embryos [63]. On the other hand, several reports have shown that BM-derived cells migrate to the corneal stroma [64, 65]. Recently, Sosnova et al. [48] reported that keratocytes do not express CD34 in the mouse corneal stroma and that all $CD34^+$ cells coexpressed CD45 and were therefore BM-derived. However, Espana et al. [39] reported CD34 expression in cultured human keratocytes. We found $CD34^+CD45^-$ cells in COP spheres (Fig. 5), which were distinct from the $CD34^+CD45^+$ adhesive cells isolated from corneas of GFP^+ WBM transplanted mice (Fig. 6). Given that GFP^+ COP spheres were not observed in GFP^+ WBM transplanted mice, COPs appear to be non-BM progenitors that express CD34, at least during sphere cultures. Furthermore, COPs prepared from Wnt1-Cre/Floxed-EGFP and P0-Cre/Floxed-EGFP mice were $EGFP^+$ (Fig. 7), strongly suggesting that these cells prepared from the cornea are of neural crest origin. Anti-GFP immunostaining also revealed neural crest-derived cells in the corneal stroma of Wnt1-Cre/Floxed-EGFP mice, with weaker levels of GFP expression in the stroma (Fig. 7B) compared with the endothelium (Fig. 7A). The weak expression of GFP in the stroma is probably due to the thin dendritic morphology of keratocytes, as well as the fact that stromal keratocytes are quiescent in vivo [66–68].

Further investigations are required to determine whether COPs are unique cells that reside in the corneal stroma or whether they represent a lineage of NSCs common with SKPs that migrate to the cornea. Although there is still controversy as to the identity of SKPs [69], the similarity of COPs with SKPs also has several clinical implications for the possible use of dermal cells for reconstructing the corneal stroma. If abundant dermal SKPs can be induced to differentiate into keratocytes, the development of corneal equivalents using autologous tissue may become a reality. Further studies to isolate COPs from humans for regenerative purposes are under way.

ACKNOWLEDGMENTS

We thank Kimie Kato for technical assistance, Hiroko Kouike for expert assistance with flow cytometric analysis, Fumito Morito for cell cultures, and Prof. Masaru Okabe (Genome Information Research Center) for providing the GFP-transgenic mice (C57BL/6 TgN [act-EGFP]OsbC14-Y01-FM131). This study was partly supported by a grant from the Advanced and Innovational Research Program in Life Sciences from the Ministry of Education, Culture, Sports, Science and Technology of Japan (to T.K. and H.O.), a grant from Core Research for Evolutional Science and Technology (CREST) of Japan Science and Technology Corporation (to H.O.), and a grant-in-aid to Keio University from the 21st Century Center of Excellence (COE) program.

DISCLOSURES

The authors indicate no potential conflicts of interest.

REFERENCES

1 Lavker RM, Tseng SC, Sun TT. Corneal epithelial stem cells at the limbus: Looking at some old problems from a new angle. Exp Eye Res 2004;78:433–446.

2 Uchida S, Yokoo S, Yanagi Y et al. Sphere formation and expression of neural proteins by human corneal stromal cells in vitro. Invest Ophthalmol Vis Sci 2005;46:1620–1625.

3 Funderburgh ML, Du Y, Mann MM et al. PAX6 expression identifies progenitor cells for corneal keratocytes. FASEB J 2005;19: 1371–1373.

4 Wilson SE, Pedroza L, Beuerman R et al. Herpes simplex virus type-1 infection of corneal epithelial cells induces apoptosis of the underlying keratocytes. Exp Eye Res 1997;64:775–779.

5 Helena MC, Baerveldt F, Kim WJ et al. Keratocyte apoptosis after corneal surgery. Invest Ophthalmol Vis Sci 1998;39:276–283.

6 Johnston MC, Noden DM, Hazelton RD et al. Origins of avian ocular and periocular tissues. Exp Eye Res 1979;29:27–43.

7 Trainor PA, Tam PP. Cranial paraxial mesoderm and neural crest cells of the mouse embryo: Co-distribution in the craniofacial mesenchyme but distinct segregation in branchial arches. Development 1995;121: 2569–2582.

8 Reynolds BA, Weiss S. Generation of neurons and astrocytes from isolated cells of the adult mammalian central nervous system. Science 1992;255:1707–1710.

9 Yoshida S, Shimmura S, Shimazaki J et al. Serum-free spheroid culture of mouse corneal keratocytes. Invest Ophthalmol Vis Sci 2005;46: 1653–1658.

10 Toma JG, McKenzie IA, Bagli D et al. Isolation and characterization of multipotent skin-derived precursors from human skin. STEM CELLS 2005;23:727–737.

11 Toma JG, Akhavan M, Fernandes KJ et al. Isolation of multipotent adult stem cells from the dermis of mammalian skin. Nat Cell Biol 2001;3: 778–784.

12 Fernandes KJ, McKenzie IA, Mill P et al. A dermal niche for multipotent adult skin-derived precursor cells. Nat Cell Biol 2004;6:1082–1093.

13 Danielian PS, Muccino D, Rowitch DH et al. Modification of gene activity in mouse embryos in utero by a tamoxifen-inducible form of Cre recombinase. Curr Biol 1998;8:1323–1326.

14 Yamauchi Y, Abe K, Mantani A et al. A novel transgenic technique that allows specific marking of the neural crest cell lineage in mice. Dev Biol 1999;212:191–203.

15 Kawamoto S, Niwa H, Tashiro F et al. A novel reporter mouse strain that expresses enhanced green fluorescent protein upon Cre-mediated recombination. FEBS Lett 2000;470:263–268.

16 Okabe M, Ikawa M, Kominami K et al. 'Green mice' as a source of ubiquitous green cells. FEBS Lett 1997;407:313–319.

17 Kawase Y, Yanagi Y, Takato T et al. Characterization of multipotent adult stem cells from the skin: Transforming growth factor-beta (TGF-beta) facilitates cell growth. Exp Cell Res 2004;295:194–203.

18 Suslov ON, Kukekov VG, Ignatova TN et al. Neural stem cell heterogeneity demonstrated by molecular phenotyping of clonal neurospheres. Proc Natl Acad Sci U S A 2002;99:14506–14511.

19 Ignatova TN, Kukekov VG, Laywell ED et al. Human cortical glial tumors contain neural stem-like cells expressing astroglial and neuronal markers in vitro. Glia 2002;39:193–206.

20 Laywell ED, Rakic P, Kukekov VG et al. Identification of a multipotent astrocytic stem cell in the immature and adult mouse brain. Proc Natl Acad Sci U S A 2000;97:13883–13888.

21 Kukekov VG, Laywell ED, Suslov O et al. Multipotent stem/progenitor cells with similar properties arise from two neurogenic regions of adult human brain. Exp Neurol 1999;156:333–344.

22 Gritti A, Frolichsthal-Schoeller P, Galli R et al. Epidermal and fibroblast growth factors behave as mitogenic regulators for a single multipotent stem cell-like population from the subventricular region of the adult mouse forebrain. J Neurosci 1999;19:3287–3297.

23 Kukekov VG, Laywell ED, Thomas LB et al. A nestin-negative precursor cell from the adult mouse brain gives rise to neurons and glia. Glia 1997;21:399–407.

24 Keller G, Kennedy M, Papayannopoulou T et al. Hematopoietic commitment during embryonic stem cell differentiation in culture. Mol Cell Biol 1993;13:473–486.

25 Kawaguchi A, Miyata T, Sawamoto K et al. Nestin-EGFP transgenic mice: Visualization of the self-renewal and multipotency of CNS stem cells. Mol Cell Neurosci 2001;17:259–273.

26 Kaneko Y, Sakakibara S, Imai T et al. Musashi1: An evolutionally conserved marker for CNS progenitor cells including neural stem cells. Dev Neurosci 2000;22:139–153.

27 Murayama A, Matsuzaki Y, Kawaguchi A et al. Flow cytometric analysis of neural stem cells in the developing and adult mouse brain. J Neurosci Res 2002;69:837–847.

28 Shukunami C, Shigeno C, Atsumi T et al. Chondrogenic differentiation of clonal mouse embryonic cell line ATDC5 in vitro: Differentiation-dependent gene expression of parathyroid hormone (PTH)/PTH-related peptide receptor. J Cell Biol 1996;133:457–468.

29 Sakakibara S, Nakamura Y, Yoshida T et al. RNA-binding protein Musashi family: Roles for CNS stem cells and a subpopulation of ependymal cells revealed by targeted disruption and antisense ablation. Proc Natl Acad Sci U S A 2002;99:15194–15199.

30 Sakakibara S, Okano H. Expression of neural RNA-binding proteins in the postnatal CNS: Implications of their roles in neuronal and glial cell development. J Neurosci 1997;17:8300–8312.

31 Sawamoto K, Yamamoto A, Kawaguchi A et al. Direct isolation of committed neuronal progenitor cells from transgenic mice coexpressing spectrally distinct fluorescent proteins regulated by stage-specific neural promoters. J Neurosci Res 2001;65:220–227.

32 Reya T, Morrison SJ, Clarke MF et al. Stem cells, cancer, and cancer stem cells. Nature 2001;414:105–111.

33 Kobayashi M, Sjoberg G, Soderhall S et al. Pediatric rhabdomyosarcomas express the intermediate filament nestin. Pediatr Res 1998;43: 386–392.

34 Staud F, Pavek P. Breast cancer resistance protein (BCRP/ABCG2). Int J Biochem Cell Biol 2005;37:720–725.

35 Blanpain C, Lowry WE, Geoghegan A et al. Self-renewal, multipotency, and the existence of two cell populations within an epithelial stem cell niche. Cell 2004;118:635–648.

36 Morris RJ, Liu Y, Marles L et al. Capturing and profiling adult hair follicle stem cells. Nat Biotechnol 2004;22:411–417.

37 Jackson KA, Mi T, Goodell MA. Hematopoietic potential of stem cells isolated from murine skeletal muscle. Proc Natl Acad Sci U S A 1999; 96:14482–14486.

38 Torrente Y, Tremblay JP, Pisati F et al. Intraarterial injection of muscle-derived CD34(+)Sca-1(+) stem cells restores dystrophin in mdx mice. J Cell Biol 2001;152:335–348.

39 Espana EM, Kawakita T, Liu CY et al. CD-34 expression by cultured human keratocytes is downregulated during myofibroblast differentiation induced by TGF-beta1. Invest Ophthalmol Vis Sci 2004;45:2985–2991.

40 Ito CY, Li CY, Bernstein A et al. Hematopoietic stem cell and progenitor defects in Sca-1/Ly-6A-null mice. Blood 2003;101:517–523.

41 Welm BE, Tepera SB, Venezia T et al. Sca-1(pos) cells in the mouse mammary gland represent an enriched progenitor cell population. Dev Biol 2002;245:42–56.

42 Satoh M, Mioh H, Shiotsu Y et al. Mouse bone marrow stromal cell line MC3T3-G2/PA6 with hematopoietic-supporting activity expresses high levels of stem cell antigen Sca-1. Exp Hematol 1997;25:972–979.

43 Richardson GD, Robson CN, Lang SH et al. CD133, a novel marker for human prostatic epithelial stem cells. J Cell Sci 2004;117:3539–3545.

44 Corbeil D, Roper K, Hellwig A et al. The human AC133 hematopoietic stem cell antigen is also expressed in epithelial cells and targeted to plasma membrane protrusions. J Biol Chem 2000;275:5512–5520.

45 Uchida N, Buck DW, He D et al. Direct isolation of human central nervous system stem cells. Proc Natl Acad Sci U S A 2000;97:14720–14725.

46 Belicchi M, Pisati F, Lopa R et al. Human skin-derived stem cells migrate throughout forebrain and differentiate into astrocytes after injection into adult mouse brain. J Neurosci Res 2004;77:475–486.

47 Jackson KA, Majka SM, Wulf GG et al. Stem cells: A minireview. J Cell Biochem Suppl 2002;38:1–6.

48 Sosnova M, Bradl M, Forrester JV. $CD34^+$ corneal stromal cells are bone marrow-derived and express hemopoietic stem cell markers. STEM CELLS 2005;23:507–515.

49 Hermann A, Gastl R, Liebau S et al. Efficient generation of neural stem cell-like cells from adult human bone marrow stromal cells. J Cell Sci 2004;117:4411–4422.

50 Anjos-Afonso F, Siapati EK, Bonnet D. In vivo contribution of murine mesenchymal stem cells into multiple cell-types under minimal damage conditions. J Cell Sci 2004;117:5655–5664.

51 Tomita Y, Matsumura K, Wakamatsu Y et al. Cardiac neural crest cells contribute to the dormant multipotent stem cell in the mammalian heart. J Cell Biol 2005;170:1135–1146.

52 Cvekl A, Tamm ER. Anterior eye development and ocular mesenchyme: New insights from mouse models and human diseases. Bioessays 2004; 26:374–386.

53 Gage PJ, Rhoades W, Prucka SK et al. Fate maps of neural crest and mesoderm in the mammalian eye. Invest Ophthalmol Vis Sci 2005;46: 4200–4208.

54 Molofsky AV, Pardal R, Iwashita T et al. Bmi-1 dependence distinguishes neural stem cell self-renewal from progenitor proliferation. Nature 2003;425:962–967.

55 Du Y, Funderburgh ML, Mann MM et al. Multipotent stem cells in human corneal stroma. STEM CELLS 2005;23:1266–1275.

56 Wroblewski J, Engstrom M, Edwall-Arvidsson C et al. Distribution of nestin in the developing mouse limb bud in vivo and in micro-mass cultures of cells isolated from limb buds. Differentiation 1997;61: 151–159.

57 Mignone JL, Kukekov V, Chiang AS et al. Neural stem and progenitor cells in nestin-GFP transgenic mice. J Comp Neurol 2004;469:311–324.

58 Zimmerman L, Parr B, Lendahl U et al. Independent regulatory elements in the nestin gene direct transgene expression to neural stem cells or muscle precursors. Neuron 1994;12:11–24.

59 Lothian C, Lendahl U. An evolutionarily conserved region in the second intron of the human nestin gene directs gene expression to CNS progenitor cells and to early neural crest cells. Eur J Neurosci 1997;9:452–462.

60 Kayahara T, Sawada M, Takaishi S et al. Candidate markers for stem and early progenitor cells, Musashi-1 and Hes1, are expressed in crypt base columnar cells of mouse small intestine. FEBS Lett 2003;535:131–135.

61 Potten CS, Booth C, Tudor GL et al. Identification of a putative intestinal stem cell and early lineage marker; musashi-1. Differentiation 2003;71: 28–41.

62 Clarke RB, Spence K, Anderson E et al. A putative human breast stem cell population is enriched for steroid receptor-positive cells. Dev Biol 2005;277:443–456.

63 Lwigale PY, Cressy PA, Bronner-Fraser M. Corneal keratocytes retain neural crest progenitor cell properties. Dev Biol 2005;288:284–293.

64 Nakamura T, Ishikawa F, Sonoda KH et al. Characterization and distribution of bone marrow-derived cells in mouse cornea. Invest Ophthalmol Vis Sci 2005;46:497–503.

65 Hamrah P, Liu Y, Zhang Q et al. The corneal stroma is endowed with a significant number of resident dendritic cells. Invest Ophthalmol Vis Sci 2003;44:581–589.

66 Beales MP, Funderburgh JL, Jester JV et al. Proteoglycan synthesis by bovine keratocytes and corneal fibroblasts: Maintenance of the keratocyte phenotype in culture. Invest Ophthalmol Vis Sci 1999;40: 1658–1663.

67 Jester JV, Barry PA, Lind GJ et al. Corneal keratocytes: In situ and in vitro organization of cytoskeletal contractile proteins. Invest Ophthalmol Vis Sci 1994;35:730–743.

68 West-Mays JA, Dwivedi DJ. The keratocyte: Corneal stromal cell with variable repair phenotypes. Int J Biochem Cell Biol 2006;38:1625–1631.

69 Rendl M, Lewis L, Fuchs E. Molecular dissection of mesenchymal-epithelial interactions in the hair follicle. PLoS Biol 2005;3:e331.

See www.StemCells.com for supplemental material available online.

Proliferation and Differentiation of Transplantable Rabbit Epithelial Sheets Engineered with or without an Amniotic Membrane Carrier

Kazunari Higa,[1] *Shigeto Shimmura,*[1,2] *Naoko Kato,*[2] *Tetsuya Kawakita,*[1] *Hideyuki Miyashita,*[2] *Yuji Itabashi,*[3] *Keiichi Fukuda,*[3] *Jun Shimazaki,*[1,2] *and Kazuo Tsubota*[1,2]

Purpose. To report a novel method of engineering transplantable, carrier-free corneal epithelial sheets by using a biodegradable fibrin sealant and to compare its characteristics with epithelial sheets cultivated on denuded amniotic membrane carriers.

Methods. Stratified corneal epithelial sheets were prepared in culture dishes coated with biodegradable fibrin glue. Amniotic membrane (AM) carriers served as the control. The quality of cultivated sheets was compared by immunohistochemistry for cytokeratin (K)3, K12, K14, p63, occludin, and integrin β1; electron microscopy; and colony-forming assays. K3 protein expression was compared by Western blot analysis. In a limbal-deficient rabbit transplantation model, postoperative adaptation and proliferation of BrdU-labeled cell sheets were examined by histology and anti-Ki67 staining.

Results. Epithelial sheets were successfully engineered by using a biodegradable fibrin sealant. Cell sheets in both groups were multilayered, expressed K3, K12, and K14, and had functioning occludin$^+$ apical tight junctions as well as p63 and integrin β1 staining in basal cells. The carrier-free sheets appeared to be more differentiated than the AM sheets, which was also demonstrated by the higher levels of K3 in the Western blots. The colony-forming efficiency of dissociated cells was similar in both groups, although larger colonies were observed on the AM sheets. AM sheets retained higher levels of BrdU-labeled cells and fewer Ki67$^+$ cells compared with carrier-free sheets after transplantation.

Conclusions. Tissue engineering with a commercially available fibrin sealant was an effective means of creating a carrier-free, transplantable corneal epithelial sheet. Carrier-free sheets were more differentiated compared with AM sheets, while retaining similar levels of colony-forming progenitor cells. (*Invest Ophthalmol Vis Sci.* 2007;48:597–604) DOI:10.1167/iovs.06-0664

From the [1]Department of Ophthalmology, Tokyo Dental College, Chiba, Japan; and the Departments of [2]Ophthalmology and [3]Regenerative Medicine and Advanced Cardiac Therapeutics, Keio University School of Medicine, Tokyo, Japan.

Supported in part by a grant from Advanced and Innovational Research Program in Life Sciences from the Ministry of Education, Culture, Sports, Science and Technology (TK) and a Grant-in-Aid for Scientific Research (SS).

Submitted for publication June 15, 2006; revised September 22, 2006; accepted December 14, 2006.

Disclosure: **K. Higa**, None; **S. Shimmura**, None; **N. Kato**, None; **T. Kawakita**, None; **H. Miyashita**, None; **Y. Itabashi**, None; **K. Fukuda**, None; **J. Shimazaki**, None; **K. Tsubota**, None

The publication costs of this article were defrayed in part by page charge payment. This article must therefore be marked "*advertisement*" in accordance with 18 U.S.C. §1734 solely to indicate this fact.

Corresponding author: Shigeto Shimmura, Department of Ophthalmology, Keio University School of Medicine, 35 Shinanomachi, Shinjuku-ku, Tokyo 160-8582, Japan; shige@sc.itc.keio.ac.jp.

Investigative Ophthalmology & Visual Science, February 2007, Vol. 48, No. 2

The use of allogenic or autologous cell sources for regenerative surgery is already common practice in the reconstruction of the ocular surface in patients with stem cell deficiency.[1,2] After the success of limbal transplantation, a second generation of regenerative corneal surgery has emerged in the form of cell sheet transplantation by tissue-engineering techniques.[3] Cell sheet transplants currently in clinical use are prepared by using biological carriers such as fibrin[4] or amniotic membrane (AM)[5–7] or as carrier-free cell sheets.[8,9] Although there is still debate as to whether the cultivated sheets include progenitor or stem cells, both carrier and carrier-free techniques have restored a clear ocular surface for at least 1 year, the empiric goal for successful stem cell surgery.[7,9]

One of the major benefits of cell sheet transplants, is that it can avoid the problem of donor availability. In vitro expansion provides a stratified cell sheet suitable for transplantation from a millimeter-scale tissue source procured from the healthy eye of the same patient or from a living relative in the case of bilateral disease. Ectopic cell sources such as the buccal membrane can also be modified in vitro to form a stratified epithelial sheet for ocular surface reconstruction with autologous tissue.[9–11] Yet, the number of clinical cases has not met the needs of patients because of ethical and technical constraints. Using AM as a carrier is one possibility as a standardized technique to produce transplantable epithelial sheets; however, AM tissue may not be readily available.

The development of a carrier-free method to produce corneal epithelial sheets was first reported by Nishida et al.,[8] who used a novel temperature-responsive polymer that changes molecular conformation and hydrophobicity at 20°C to release intact sheets. Clinical cases in which this technique has been used have shown that a carrier-free strategy is feasible and that transplantation can be performed without the use of sutures. In the present study, we developed a different technique by using commercially available fibrin sealants to produce carrier-free sheets. Our method is different from the fibrin carrier sheets described by Rama et al.,[4] as we allowed the fibrin to be degraded by intrinsic proteases before transplantation.

Materials and Methods

Antibodies

Mouse monoclonal antibodies (mAbs) for cytokeratin (K)3, K14, laminin, p63, integrin β1, and Ki67 were purchased from Progen (AE5; Heidelberg, German), Abcam (B429; Cambridgeshire, UK), Laboratory Vision (4C7; Fremont, CA), Calbiochem (4A4; Merck KGaA, Darmstadt, Germany), Chemicon International Inc. (LM534; Temecula, CA), and DakoCytomation (MIB-1; Glostrup, Denmark), respectively. Mouse IgM antibody for fibrin was purchased from Monosan (Uden, The Netherlands). Rabbit polyclonal antibody for K12, goat polyclonal antibody for type IV collagen and rat mAb for BrdU (ICR1) were purchased from TransGenic, Inc. (Kumamoto, Japan), Southern Biotechnology Associates, Inc. (Birmingham, AL) and Abcam. Isotype goat IgG, mouse IgG1,

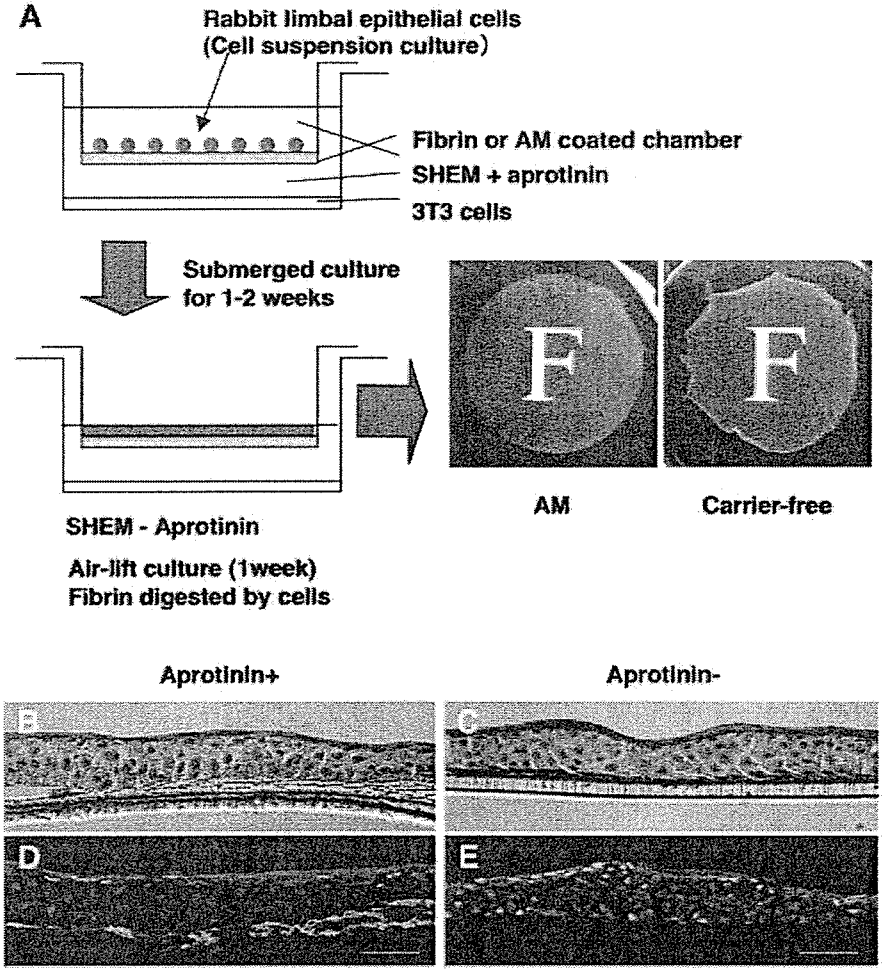

FIGURE 1. Cultivation of carrier-free epithelial sheets. Limbal epithelial cells were collected and seeded on fibrin- or AM-coated chambers (A). After 1 to 2 weeks in submerged culture with MMC-treated 3T3 feeder fibroblasts, the cells were allowed to stratify at the air–liquid interface for 1 week. HE staining (B, C) and immunohistochemistry against fibrin (*green*) and K12 (*red*) (D, E) showed that fibrin acted as a scaffold during cultivation with the protease inhibitor aprotinin (B, D) and was allowed to dissolve by removing the aprotinin before transplantation (C, E).

mouse IgM, rabbit IgG and rat IgG as control were purchased from Santa Cruz Biotechnology (Santa Cruz, CA), Dako Cytomation, and Jackson ImmunoResearch Laboratories (West Grove, PA), respectively. FITC-, rhodamine-, and Cy3-conjugated secondary antibodies were purchased from Jackson ImmunoResearch Laboratories and Chemicon International Inc.

Preparation of Epithelial Cells Sheets

All experimental procedures and protocols were approved by the Animal Care and Use Committee of Tokyo Dental College and conformed to the National Instituted of Health Guide for the Care and Use of Laboratory Animals. Fibrin scalant was purchased from Fujisawa (Bolheal; Osaka, Japan), and its constitution was performed as reported previously.[12] In brief, a solution containing 40 mg of human fibrinogen and 0.18 U of thrombin was diluted with 7.5 mL saline, and 0.3 mL was spread rapidly onto the upper chambers of a six-well plate with culture inserts (Transwell; Costar Corning, Corning, NY). Two hours later, the polymerized fibrin-coated top chambers were obtained and stored at 4°C. AMs were donated by mothers who were seronegative for human immunodeficiency virus and hepatitis B and C virus at the time of cesarean section, after written informed consent was obtained, in accordance with the Declaration of Helsinki. AM was stored with 15% dimethylsulfoxide (Sigma-Aldrich, St. Louis, MO) with PBS at −80°C until use. Denuded AM was prepared as previously described.[7] Membranes were rinsed in PBS, spread onto the upper chambers of a six-well insert, frozen at −80°C, and air-dried at room temperature.

Primary cultures of limbal epithelial cells were prepared from eyes of 2.5- to 3.0-kg female Japanese white rabbits (Japan CLEA, Tokyo, Japan) with anesthesia induced by intravenous injection of 4 mL pentobarbital sodium (50 mg/mL). Limbal rims of corneoscleral tissue were prepared by careful removal of excess sclera, iris, corneal endothelium, and central cornea. Epithelial sheets were isolated as described previously.[13] Dispersed epithelial sheets were treated with trypsin-ethylenediaminetetracetic acid (EDTA) for 10 minutes, to suspend cells, which were seeded onto fibrin- or AM-coated wells (2×10^5 cells/mL) with supplemented hormonal epithelial medium (SHEM)[7] containing 666 KIU/mL aprotinin (Wako, Osaka, Japan) and cocultured with mitomycin C (MMC)-treated 3T3 fibroblasts (Fig. 1A). The cultures were submerged in medium until confluence, cultured in air–liquid interface for 1 week, and finally incubated without aprotinin for 4 days. To evaluate the proliferation of transplanted epithelium and to identify cells of donor origin, cell sheets were labeled with 10 μM BrdU for 48 hours before surgery. After labeling with BrdU, the epithelial cell sheets were washed with fresh medium and then used for surgery.

Transmission Electron Microscopy

Epithelial cell sheets were processed for transmission electron microscopy. Epithelial cell sheets from both groups were fixed in 2.5% glutaraldehyde solution in 60 mM HEPES buffer solution for 4 hours. After washing, samples were postfixed in 1% osmium tetroxide, dehydrated in a series of ethanol and propylene oxide, and embedded in epoxy resin. Semithin sections (1-μm) were stained with toluidine blue. Then, ultrathin specimens were sectioned with a microtome (LKB, Gaithersburg, MD). Sections in the range of gray to silver were collected on 150-mesh grid, stained with uranyl acetate and lead

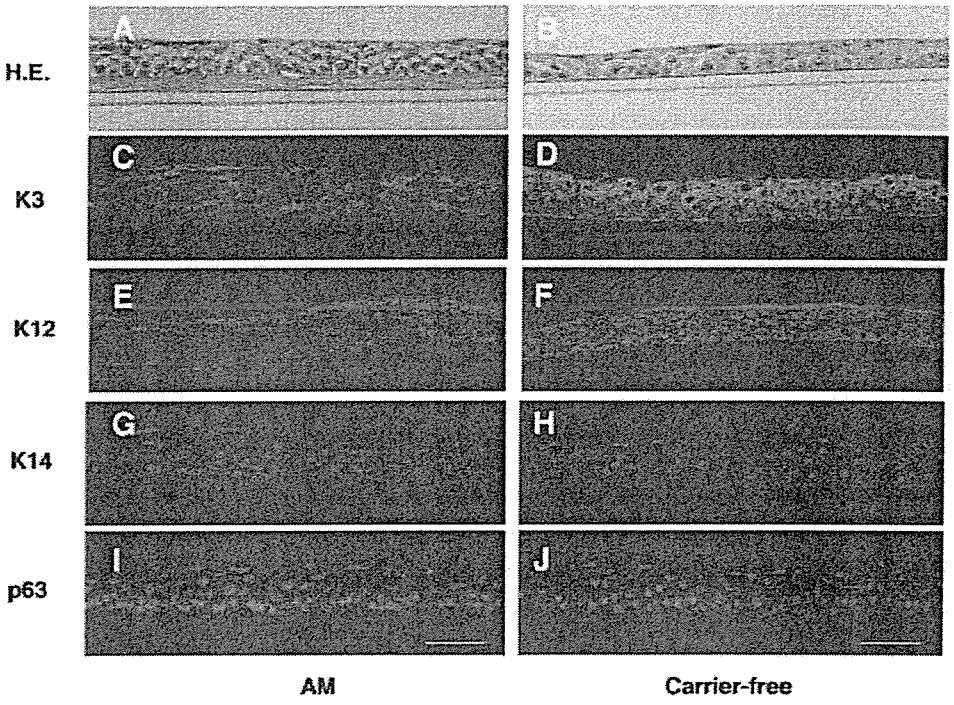

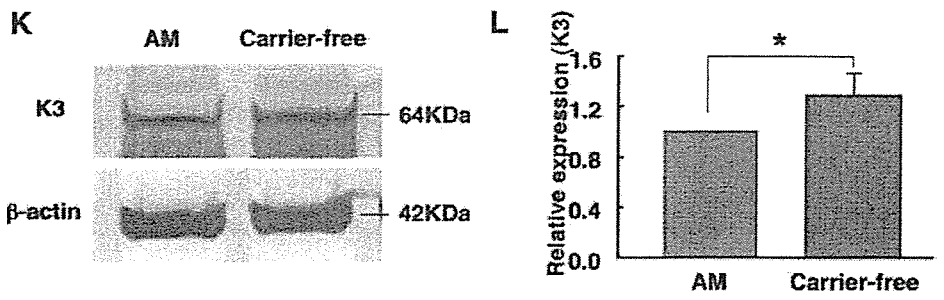

FIGURE 2. Differentiation markers in epithelial sheets. Hematoxylin and eosin staining of AM (A) and carrier-free (B) epithelial cell sheets. (C–J) Immunohistochemistry of K3, K12, K14, and p63 in epithelial sheets. Carrier-free sheets showed stronger K3/K12 staining and weaker K14/p63 staining than did AM sheets. Nuclei of cells were stained with DAPI. Scale bar, 50 μm. The difference in K3 expression was confirmed by Western blot (K), which showed significantly higher levels of K3 in carrier-free sheets than in AM sheets, when compared semiquantitatively (L, $n = 6$, $^*P = 0.002$).

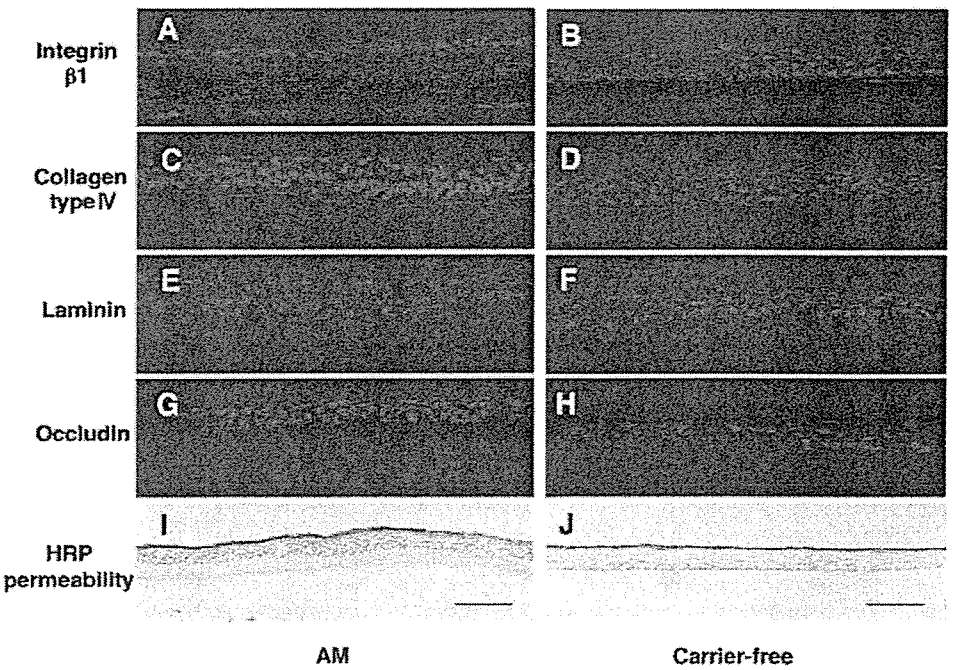

FIGURE 3. Basement membrane components and barrier function in epithelial sheets. Immunohistochemistry of integrin β1, collagen type IV, laminin, and occludin in AM (A, C, E, G) and carrier-free (B, D, F, H) epithelial sheets. Nuclei of cells were stained with DAPI. (I, J) Barrier function (HRP permeability) of the epithelial sheets. Scale bar, 50 μm.

citrate, and examined under an electron microscope (model 1200 EXII; JEOL, Tokyo, Japan).

Colony-Forming Efficiency

To evaluate the proliferative potential of cells in the cultured sheets, MMC-treated 3T3 fibroblasts were used in a colony-forming efficiency (CFE) assay, as previously described.[14–16] NIH 3T3 fibroblasts in DMEM containing 10% FCS were treated with MMC (4 μg/mL) for 2 hours at 37°C and then treated with trypsin-EDTA and plated at a density of 3×10^6 cells in 100-mm culture dishes. Single cells were prepared from both treated epithelial cell sheets (Acutase; Innovative Cell Technologies, Inc., San Diego, CA) for 60 minutes at 37°C. Each dish was seeded at 1×10^3 cells/dish. CFE was calculated by the percentage of colonies at day 14 generated by the number of epithelial cells plated in the dish. Quantification of size (in square millimeters) and number of colonies obtained from AM or fibrin sheets ($n = 5$) was performed by NIH Image (available by ftp at zippy.nimh.nih.gov/ or at http://rsb.info.nih.gov/nih-image; developed by Wayne Rasband, National Institutes of Health, Bethesda, MD). Growth capacity was evaluated on day 14 when cultured cells were stained with rhodamine B (Wako) for 30 minutes.

Epithelial Sheet Transplantation

All animals were handled in full accordance with the ARVO Statement for the Use of Animals in Ophthalmic and Vision Research and institutional guidelines. Rabbits were anesthetized with intramuscular injection of xylazine hydrochloride (2.5 mg/mL) and ketamine hydrochloride (37.5 mg/mL). The left eye in each rabbit was rendered totally limbal stem cell deficient by 1-*n*-heptanol (Sigma-Aldrich) mechanical debridement of the corneal epithelium, and surgical removal of the limbal and conjunctival epithelium was performed up to 2 mm from the limbus. Carrier-free sheets were gently detached from the mesh with a cell scraper,[12] transferred by microforceps and then expanded on the bare corneal stroma with a surgical sponge or forceps. Cell sheets were allowed to attach for 5 minutes without sutures. AM carrier sheets were sutured to the corneal surface with 10-0 nylon sutures. Rabbits with denuded corneas without sheet transplants served as the control. After surgery, all rabbits were fitted with a bandage contact lens and topical antibiotic (levofloxacin), and steroids (betamethasone) were applied twice daily.

The percentage of the cornea covered by epithelium at 1 week after surgery was calculated by measuring the area of the epithelial defects. The defect area was analyzed by tracing fluorescein images and calculated using the NIH Image program. Rabbits were then killed to observe BrdU-labeled cells as a means to confirm the donor origin of epithelium. The proliferation of transplanted epithelial cells was examined by calculating the percentage of $BrdU^+$ and $Ki67^+$ nuclei by immunohistochemistry.

Immunohistochemistry

Paraffin sections (K3, K14, p63, BrdU, and Ki67) were deparaffinized in xylene and rehydrated. Frozen sections (type IV collagen and laminin) were fixed for 10 minutes in cold acetone before blocking. Frozen sections (integrin β1 and K12) were fixed for 10 minutes in 2% paraformaldehyde (Wako). Sections were blocked by incubation with 10% normal donkey serum (Chemicon International Inc., Temecula, CA) and 1% bovine serum albumin (Sigma-Aldrich) for 1 hour at room temperature (RT). Antibodies to K3 (1:50), K12 (1:100), K14 (1:100), p63 (1:50), BrdU (1:100), Ki67 (1:50), type IV collagen (1:50), laminin (1:50), and integrin β1 (1:100) were applied and incubated for 90 minutes at RT, followed by incubation with rhodamine- or Cy3-conjugated secondary antibody. After three washes with TBST, the sections were incubated with 1 mg/mL 4′,6-diamidino-2-phenylindole (DAPI; Dojindo Laboratories, Tokyo, Japan) at RT for 5 minutes. Finally, the sections were washed three times in TBST and coverslipped after mounting with an antifade medium (50 mM Tris buffer saline, 90% glycerin; Wako), 10% 1,4-diazabicyclo-2,2,2-octane (Wako).

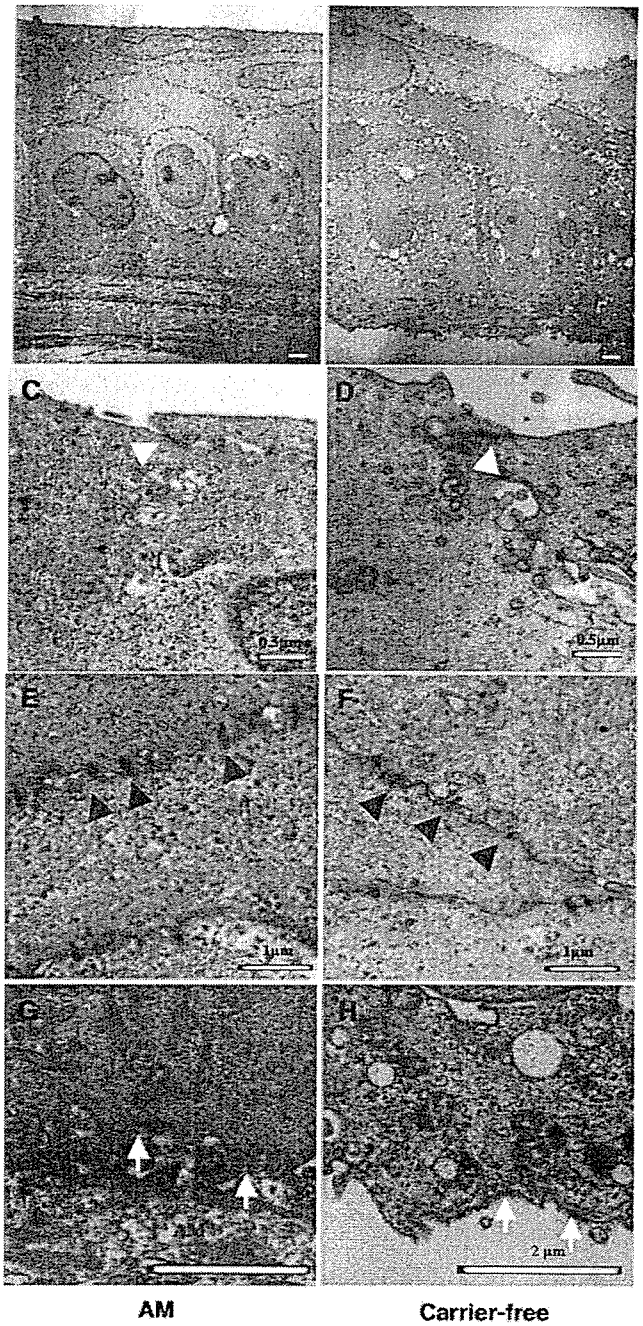

FIGURE 4. Transmission electron micrographs of AM and carrier-free sheets. Both AM (A, C, E, G) and carrier-free (B, D, F, H) sheets formed five to six layers of well-stratified epithelial cells, with columnar basal epithelial cells. High-magnification views show tight junction formation in apical cells (C, D, *white arrowheads*), and desmosome formation in the intermediate layers (E, F, *black arrowheads*). Basal cells formed an intact basement membrane in the AM sheets (G, *arrows*), whereas carrier-free sheets had residual material attached to the basal cell membrane (H, *white arrows*).

Western Blot Analysis

Epithelial sheets were dissociated with lysis buffer (50 mM Tris-HCl [pH 7.4], 150 mM NaCl, 1% Nonidet P-40; Calbiochem, Darmstadt, Germany) and homogenized. Each epithelial cell sheet was incubated for 40 minutes at 4°C, and then centrifuged at 15,000 rpm for 30 minutes at 4°C. Protein concentration of the supernatant was deter-

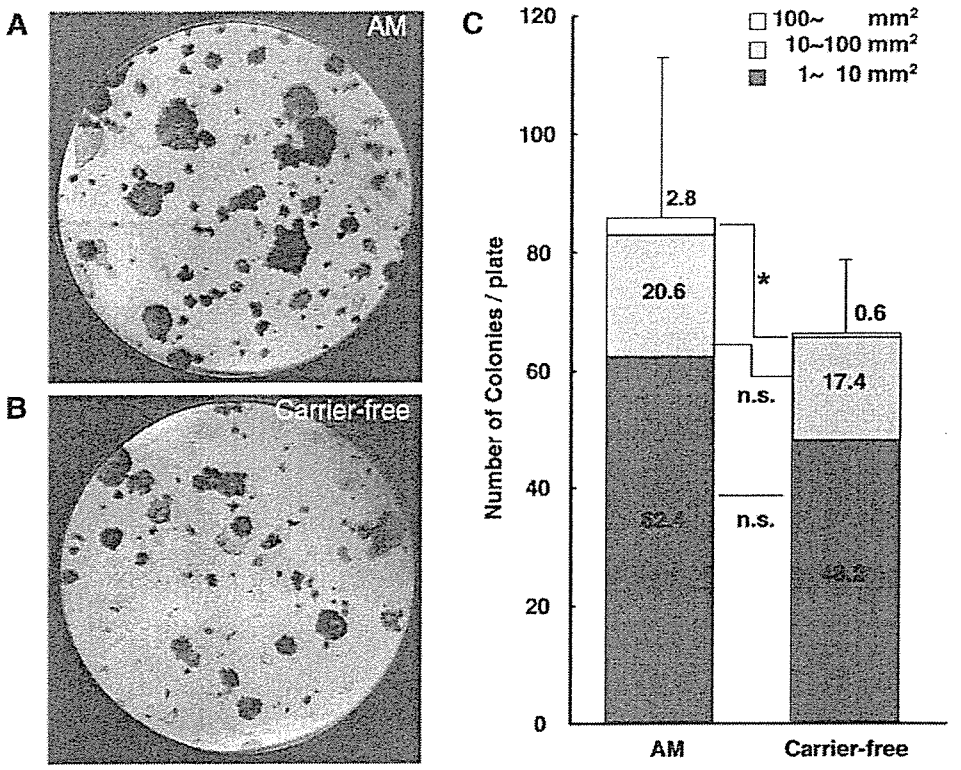

FIGURE 5. Colony formation by disassembled cells. Colony formation by epithelial cells dissociated from AM (A) and carrier-free (B) sheets. Colonies were stained with rhodamine B after 2 weeks. (C) Quantification of size and number of colonies obtained from epithelial sheets ($n = 5$, mean ± SD). There was no significant difference in total colony formation. When cultures were compared by the area of each colony, a significant difference was observed only in the largest colony size (*$P = 0.014$; Student's t-test, $n = 5$).

mined by a protein assay (DC assay; Bio-Rad Laboratory, Hercules, CA). All samples were then diluted in 2× sample buffer (100 mM Tris-HCl [pH 6.8]), 4% SDS (Invitrogen, Carlsbad, CA), 20% glycerol (Wako), 12% 2-mercaptoethanol (Wako), and boiled. Ten micrograms of each sample were loaded on a 10% Bis-Tris gel (Novex NuPAGE; Invitrogen) and transferred onto polyvinylidene difluoride (PVDF) membranes (Millipore, Billerica, MA). The membranes were blocked with 5% skim milk (Difco Laboratories, Detroit, MI), 1.5% normal goat serum, and PBS for 60 minutes at RT. The membranes were reacted with K3 (AE5) and β-actin (mabcam8226; Abcam) for 60 minutes at RT. After the membranes were washed three times in TBST, donkey biotinylated anti-mouse IgG (Jackson ImmunoResearch Laboratories) was added for 30 minutes at room temperature. Protein bands were visualized (Vectastain ABC Elite Kit; Vector Laboratories, Burlingame, CA) with DAB (Vector Laboratories) as the substrate. The plot profile of the bands was analyzed with the NIH image 1.63 software with band density of AM sheets in each group standardized at 1.0.

Statistical Analysis

Statistical comparisons of Western blot band intensity, CFE, epithelialization, and BrdU and Ki67 staining were performed with the nonpaired Student's t-test (Excel; Microsoft, Redmond, WA).

RESULTS

Generation of Carrier-Free Epithelial Cell Sheets

Rabbit corneal epithelial cells were cultured with 3T3 feeder cells for 1 to 2 weeks, followed by airlift cultures to produce stratified epithelium on plastic coated with fibrin polymer (Fig. 1A). Fibrin remained at the bottom of the cell sheet when cultured with aprotinin (Figs. 1B, 1D) and was dissolved after removal of aprotinin, presumably due to intrinsic proteolytic activity (Figs. 1C, 1E).

In Vitro Characteristics of Cultivated Sheets

We performed a comparative study of carrier-free corneal epithelial sheets with epithelial sheet cultivated on AM carriers. Stratified epithelium was engineered on both AM (Fig. 2A) and plastic coated with degradable fibrin polymer (Fig. 2B). The use of aprotinin did not affect cell growth or stratification on the AM carriers.

Immunohistochemistry using anti-K3 and K12 antibodies showed that carrier-free cultures produced uniform layers of cells expressing both differentiation markers (Figs. 2C–F). Sporadic cells in the basal layer were K3 negative, which is characteristic of immature limbal basal cells in vivo. Both AM and carrier-free sheets expressed K14 (Figs. 2G, 2H) and p63 (Figs. 2I, 2J). The epithelium on AM carriers appeared to express higher levels of K14 and p63, and less K3, K12, suggesting that the AM maintains epithelial cells in a less differentiated state. The difference in K3 expression was also demonstrated by Western blot analysis (Figs. 2K, 2L). Both AM and carrier-free sheets show an intact superficial tight junction, as shown by immunohistochemistry of occludin (Figs. 3G, 3H) and the exclusion of HRP (Figs. 3I, 3J). Basement membrane components such as collagen IV and laminin were more prominent in the AM sheet in vitro (Figs. 3C, 3E). These proteins were not as evident in the carrier-free sheets before transplantation (Figs. 3D, 3F). However, the adhesion molecule integrin β1 was expressed in both sheets (Figs. 3A, 3B).

Transmission electron microscopy revealed that the ultrastructure of the epithelium was similar between the AM and carrier-free sheets, consisting of five to six layers of stratified epithelial cells with typical columnar basal cells and superficial cells with microvilli (Figs. 4A, 4B). Both cells sheets showed tight junction formation in apical cells (Figs. 4C, 4D) and desmosome formation (Figs. 4E, 4F). Although a basement membrane structure was observed in AM sheets (Fig. 4G), the carrier-free sheets showed residual material attached to the

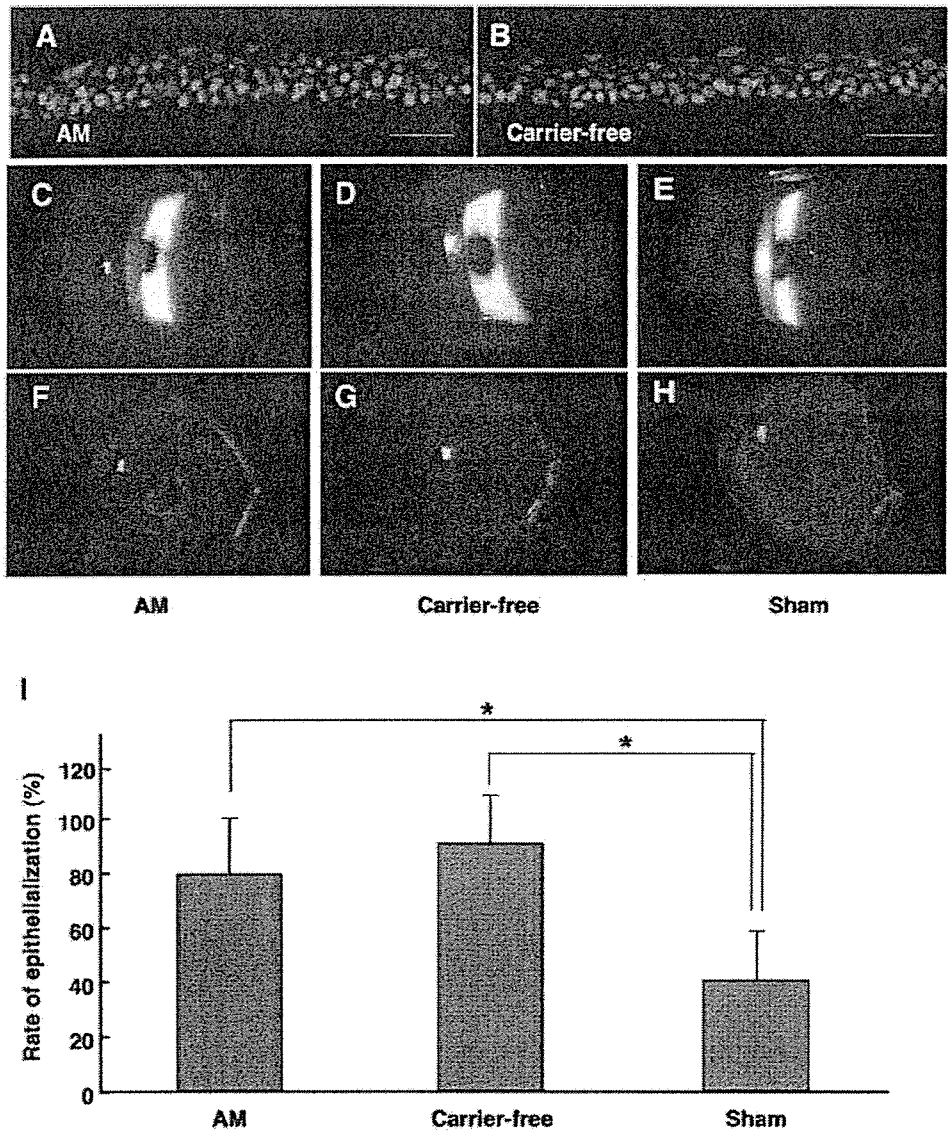

FIGURE 6. Epithelial sheet transplantation in rabbits. Immunohistochemistry of BrdU (**A**, **B**) in epithelial sheets before transplantation. Slit lamp photographs (**C**–**E**) and fluorescein staining (**F**–**H**) of rabbit eyes 1 week after epithelial sheet transplantation. (**C**, **F**) AM, (**D**, **G**) carrier-free, (**E**, **H**) sham. (**I**) Area of intact epithelium was larger in rabbit eyes after epithelial sheet transplantation compared with sham (*$P < 0.05$). Carrier-free sheets had a smoother epithelial surface with minimal inflammation. Scale bar, 50 μm.

basal epithelial membrane (Fig. 4H) which may represent components of the basement membrane structure such as integrin β1, collagen IV, and laminin observed by immunohistochemistry (Figs. 3B, 3D, 3F).

Colony-Forming Efficiency

Isolated epithelial cells from both carrier-free (6.6% ± 1.2%) and AM carrier sheets (8.6% ± 2.7%) maintained the ability to form colonies in a 3T3 feeder layer (Figs. 5A, 5B). Although the number of large colonies (100 mm^2) was higher in AM sheets (AM: 2.8 ± 1.3 colonies, fibrin: 0.6 ± 0.8 colonies, $P = 0.014$, $n = 5$), the difference in the total number of colonies was not statistically significant (Fig. 5C).

Cultivated Sheet Transplantation

BrdU labeling was performed on the AM (Fig. 6A) and carrier-free (Fig. 6B) sheets before surgery, showing that most of the cells in both groups are viable with proliferative potential. Rabbits without cell sheet transplants characteristically had epithelial defects at 1 week after surgery, as shown by the positive staining with fluorescein dye in Figure 6H (dotted line). An intact epithelial layer excluded the dye in the AM (Fig. 6F) and carrier-free (Fig. 6G) sheet transplants. The irregular staining in the AM sheet corresponds to folds in the transplant. Optical clarity was higher in the carrier-free group (Fig. 6D) than in the group with AM sheet transplants (Fig. 6C). Rabbits in the AM sheet group also had inflammation of the conjunctiva due to the presence of sutures. The area of intact epithelium at 1 week after surgery was significantly higher in both AM (79.4% ± 20.4%) and carrier-free (90.7% ± 17.4%) epithelial sheet groups compared with the sham-surgery control (40.2% ± 18.3%, $P < 0.05$; Fig. 6I).

Immunohistochemistry of postoperative corneas showed normal K3 expression in the transplant sheets (Figs. 7C, 7D). Sham-surgery eyes exhibited partial epithelialization by K3-negative epithelium of conjunctival origin. Basement membrane components such as collagen IV were more prominent in the AM sheet group (Figs. 7E, 7F). Proliferation of transplanted cells was observed by the distribution of BrdU staining, which was uniformly present in cells before surgery. BrdU-positive cells were observed in both groups, indicating that these cells were of donor origin and were slow cycling during the 1-week period after surgery (Figs. 7G, 7H). The number of BrdU-positive cells in the AM group was significantly higher

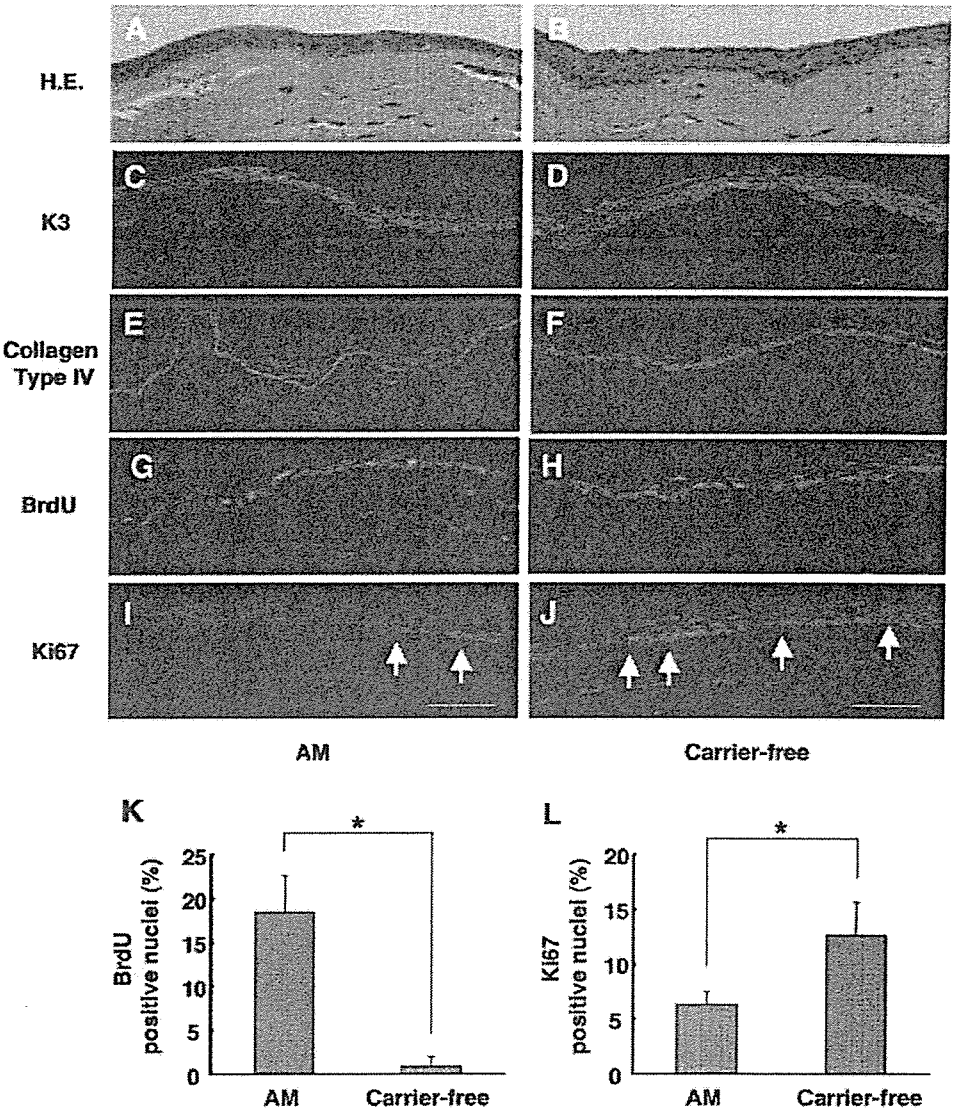

FIGURE 7. Postoperative histology of epithelial sheet transplantation. Light micrograph of hematoxylin and eosin–stained sections of AM (**A**) and carrier-free (**B**) epithelial sheets. Immunohistochemistry of K3 (**C**, **D**), Collagen type IV (**E**, **F**), BrdU (**G**, **H**), and Ki67 (**I**, **J**). AM sheets retained significantly higher levels of BrdU (**K**) and expressed lower levels of Ki67 (**L**) than did carrier-free sheets (*$P < 0.05$, Student's *t*-test). Scale bar, 50 μm.

than that in the fibrin group (AM: 18.4% ± 4.2%, fibrin: 1.1% ± 1.1%, $P = 0.0002$, $n = 4$; Fig. 7K). Staining of the proliferation marker Ki67 was also observed in the basal layers of both groups (Figs. 7I, 7J), with significantly less Ki67-positive cells in the AM group than in the fibrin group (AM: 6.3% ± 1.2%, fibrin: 12.6% ± 3.1%, $P = 0.0087$, $n = 4$; Fig. 7L). BrdU- and Ki67-positive cells were uniformly distributed throughout the epithelial sheet in both groups, and there was no tendency of higher localization of label retaining cells in the limbus under the conditions of the study.

DISCUSSION

The homeostasis of cells undergoing constant turnover depends on the healthy supply of regenerating cells, as well as an intact interaction between surrounding tissues. In the case of the corneal epithelium, stem cells in the basal limbus supply transient amplifying (TA) cells to the corneal basal layer, which proliferate and slough off the ocular surface after approximately 2 weeks. The proliferation and differentiation of epithelial cells is regulated by stromal–epithelial interaction with keratocytes, the major mesenchymal cell in the corneal stroma. Chemokines and growth factors secreted by keratocytes are involved in the proliferation and differentiation of the overlying epithelium.[17] We found that although both AM sheets and carrier-free sheets were viable in transplant-recipient eyes, carrier-free transplants demonstrated a more robust layer of fully differentiated cells.

We observed more BrdU labeled cells and fewer Ki67-labeled cells in AM sheets compared with carrier-free sheets after transplantation. Previous studies have shown that cell-cycle kinetics and cell phenotype characteristic of limbal epithelial progenitor cells are preserved during ex vivo expansion on AM.[18,19] The difference in cell-cycle kinetics may be due to the presence of the AM basement membrane, which may modulate epithelial cell adhesion, proliferation, and differentiation.[18,20,21] In contrast, epithelial cells in carrier-free sheets seem to become integrated into the host tissue earlier, suggesting that the AM may be interfering with interactions between the epithelium and stromal cells. The absence of a carrier will restore epithelium–stromal interactions immediately after surgery, may have several advantages in maintaining a healthy epithelium, and may also allow the regeneration of a normal subepithelial nerve plexus. It can be argued that a larger yield of undifferentiated cells may be preferable in the treatment of stem cell–depleted cases. However, a mature corneal epithe-

lium is also required for the ocular surface to act as a barrier against invading organisms, as well as to provide a smooth surface for visual clarity. The clinical data available to date show that both AM sheets and carrier-free sheets can restore the epithelium for more than 1 year,[7,9] which would not be possible without the restoration of progenitor cells.

Another major benefit of carrier-free cell sheets is the surgical technique, which does not require the use of sutures for donor fixation. The mechanisms involved may be multiple, however, Nishida et al.[8] show that intact basement membrane substrates and adhesion molecules may play a major role. We have confirmed the presence of β1 integrin in the carrier-free group, which may have aided the carrier-free sheets in remaining on the ocular surface without sloughing off. In contrast, AM sheets require sutures for transplantation, and ingrowth of cells was observed under the AM carrier in several cases. These results show that attachment of cell sheets to the underlying stroma is stronger with carrier-free sheets during the early postoperative stage. Furthermore, the method we describe for engineering carrier-free sheets is different from previous approaches involving temperature-responsive dishes and does not require any specialized equipment or high levels of technical expertise.

The design of our study made use of rabbits with denuded epithelium, including the limbal area. We did not take into account any damage to the underlying stromal tissue, which is sometimes observed in clinical cases after severe chemical and thermal burns. The conclusions drawn from our study therefore should be interpreted as being based on epithelial sheet transplantation in situations with relatively intact stromal tissue. The AM is rich in basement membrane components since the amnion itself supports epithelial cells in the uterus. The use of an AM carrier may therefore have benefits in cases with extensive damage and inflammation in the underlying stroma.

There are still several issues to be resolved before the generalization of epithelial sheet surgery. The manufacture of stratified epithelial sheets requires the use of 3T3 feeder cells and culture-grade serum. Although adverse effects have not been reported, xeno-free techniques should be pursued. Similarly, the choice of whether to use carriers or not requires elucidation. Our data clearly show that cell sheets engineered without carriers reconstruct host tissue nearly to its original state as early as 1 week after surgery. Further refinements in surgical technique and quality control of cultured sheets should expand the therapeutic indications for tissue-engineered cell sheet transplantation.

Acknowledgments

The authors thank Mifuyu Oshima and Tomomi Sekiguchi for technical assistance and the staff of the Cornea Center Eye Bank for administrative support.

References

1. Kenyon KR, Tseng SC. Limbal autograft transplantation for ocular surface disorders. *Ophthalmology.* 1989;96:709–722; discussion 722–723.
2. Tsubota K, Satake Y, Kaido M, et al. Treatment of severe ocular-surface disorders with corneal epithelial stem-cell transplantation. *N Engl J Med.* 1999;340:1697–1703.
3. Pellegrini G, Traverso CE, Franzi AT, et al. Long-term restoration of damaged corneal surfaces with autologous cultivated corneal epithelium. *Lancet.* 1997;349:990–993.
4. Rama P, Bonini S, Lambiase A, et al. Autologous fibrin-cultured limbal stem cells permanently restore the corneal surface of patients with total limbal stem cell deficiency. *Transplantation.* 2001;72:1478–1485.
5. Koizumi N, Inatomi T, Quantock AJ, et al. Amniotic membrane as a substrate for cultivating limbal corneal epithelial cells for autologous transplantation in rabbits. *Cornea.* 2000;19:65–71.
6. Tsai RJ, Li LM, Chen JK. Reconstruction of damaged corneas by transplantation of autologous limbal epithelial cells. *N Engl J Med.* 2000;343:86–93.
7. Shimazaki J, Aiba M, Goto E, et al. Transplantation of human limbal epithelium cultivated on amniotic membrane for the treatment of severe ocular surface disorders. *Ophthalmology.* 2002;109:1285–1290.
8. Nishida K, Yamato M, Hayashida Y, et al. Functional bioengineered corneal epithelial sheet grafts from corneal stem cells expanded ex vivo on a temperature-responsive cell culture surface. *Transplantation.* 2004;77:379–385.
9. Nishida K, Yamato M, Hayashida Y, et al. Corneal reconstruction with tissue-engineered cell sheets composed of autologous oral mucosal epithelium. *N Engl J Med.* 2004;351:1187–1196.
10. Nakamura T, Endo K, Cooper LJ, et al. The successful culture and autologous transplantation of rabbit oral mucosal epithelial cells on amniotic membrane. *Invest Ophthalmol Vis Sci.* 2003;44:106–116.
11. Nakamura T, Inatomi T, Sotozono C, et al. Transplantation of cultivated autologous oral mucosal epithelial cells in patients with severe ocular surface disorders. *Br J Ophthalmol.* 04;88:1280–1284.
12. Itabashi Y, Miyoshi S, Kawaguchi H, et al. A new method for manufacturing cardiac cell sheets using fibrin-coated dishes and its electrophysiological studies by optical mapping. *Artif Organs.* 2005;29:95–103.
13. Espana EM, Romano AC, Kawakita T, et al. Novel enzymatic isolation of an entire viable human limbal epithelial sheet. *Invest Ophthalmol Vis Sci.* 2003;44:4275–4281.
14. Kim HS, Jun Song X, de Paiva CS, et al. Phenotypic characterization of human corneal epithelial cells expanded ex vivo from limbal explant and single cell cultures. *Exp Eye Res.* 2004;79:41–49.
15. Li DQ, Chen Z, Song XJ, et al. Partial enrichment of a population of human limbal epithelial cells with putative stem cell properties based on collagen type IV adhesiveness. *Exp Eye Res.* 2005;80:581–590.
16. Tseng SC, Kruse FE, Merritt J, Li DQ. Comparison between serum-free and fibroblast-cocultured single-cell clonal culture systems: evidence showing that epithelial anti-apoptotic activity is present in 3T3 fibroblast-conditioned media. *Curr Eye Res.* 1996;15:973–984.
17. Wilson SE, Mohan RR, Mohan RR, et al. The corneal wound healing response: cytokine-mediated interaction of the epithelium, stroma, and inflammatory cells. *Prog Retin Eye Res.* 2001;20:625–637.
18. Grueterich M, Espana E, Tseng SC. Connexin 43 expression and proliferation of human limbal epithelium on intact and denuded amniotic membrane. *Invest Ophthalmol Vis Sci.* 2002;43:63–71.
19. Meller D, Pires RT, Tseng SC. Ex vivo preservation and expansion of human limbal epithelial stem cells on amniotic membrane cultures. *Br J Ophthalmol.* 2002;86:463–471.
20. Jones PH, Harper S, Watt FM. Stem cell patterning and fate in human epidermis. *Cell.* 1995;80:83–93.
21. Li W, He H, Kuo CL, et al. Basement membrane dissolution and reassembly by limbal corneal epithelial cells expanded on amniotic membrane. *Invest Ophthalmol Vis Sci.* 2006;47:2381–2389.

Available online at www.sciencedirect.com
ScienceDirect
Biochemical and Biophysical Research Communications 350 (2006) 315–321
BBRC
www.elsevier.com/locate/ybbrc

Loss of HB-EGF in smooth muscle or endothelial cell lineages causes heart malformation

Daisuke Nanba [a,1], Yumi Kinugasa [a,1], Chie Morimoto [a], Michiko Koizumi [a], Hisako Yamamura [c], Katsuhito Takahashi [c], Nobuyuki Takakura [d], Eisuke Mekada [e], Koji Hashimoto [b], Shigeki Higashiyama [a,f,*]

[a] *Department of Biochemistry and Molecular Genetics, Ehime University Graduate School of Medicine, Shitsukawa, To-on, Ehime 791-0295, Japan*
[b] *Department of Dermatology, Ehime University Graduate School of Medicine, Shitsukawa, To-on, Ehime 791-0295, Japan*
[c] *Department of Medicine, Osaka Medical Center for Cancer and Cardiovascular Diseases, Osaka 537-8511, Japan*
[d] *Department of Signal Transduction, Research Institute for Microbial Diseases, Osaka University, Osaka 565-0871, Japan*
[e] *Department of Cell Biology, Research Institute for Microbial Diseases, Osaka University, Osaka 565-0871, Japan*
[f] *PRESTO, JST, Japan*

Received 22 August 2006
Available online 22 September 2006

Abstract

Epidermal growth factor (EGF) and ErbB family molecules play a role in heart development and function. To investigate the role of EGF family member, heparin-binding EGF-like growth factor (HB-EGF) in heart development, smooth muscle and endothelial cell lineage-specific HB-EGF knockout mice were generated using the Cre/*loxP* system in combination with the *SM22α* or *TIE2* promoter. HB-EGF knockout mice displayed enlarged heart valves, and over half of these mice died during the first postnatal week, while survivors showed cardiac hypertrophy. These results suggest that expression of HB-EGF in smooth muscle and/or endothelial cell lineages is essential for proper heart development and function in mice.

Keywords: Cardiac hypertrophy; Conditional knockout; HB-EGF; Heart valves; Heart failure

Heparin-binding EGF-like growth factor (HB-EGF) is a member of the EGF family of molecules that was first identified in the conditioned media of macrophage-like U-937 cells [1]. HB-EGF is initially synthesized as a type I transmembrane precursor protein (proHB-EGF) that is subsequently enzymatically cleaved to release a soluble form of HB-EGF [1,2]. Further, HB-EGF acts as a mitogen in many different cell types and is involved in a variety of physiological and pathological processes [3–5].

Two independent studies have reported that over half of HB-EGF-null mice die before weaning and that survivors have dysfunctional hearts with grossly enlarged ventricular chambers and reduced life spans [6,7]. Moreover, studies have described the development of enlarged cardiac valves in HB-EGF-deficient mice. This heart valve enlargement has also been observed in EGF receptor (EGFR)-null mice with a CD1 background, in mice with a mutant EGFR (*waved-2*) [8], and in disintegrin and metalloprotease (ADAM) 17-null mice [7], which is a sheddase of proHB-EGF [9,10]. These results indicate that ectodomain shedding of proHB-EGF and subsequent EGFR activation induced by released HB-EGF are crucial for heart valve formation in developmental process as well as development of cardiac hypertrophy in pathological process [11]. However, it is not clear in which of the specific heart cell types (e.g., cardiac myocytes, endothelial cells, and fibroblasts) that HB-EGF expression is required for proper heart development and function.

* Corresponding author. Fax: +81 89 960 5256.
E-mail address: shigeki@m.ehime-u.ac.jp (S. Higashiyama).
[1] These authors contributed equally to this work.

0006-291X/$ - see front matter © 2006 Elsevier Inc. All rights reserved.
doi:10.1016/j.bbrc.2006.09.060

To address this issue, the present study utilized the Cre/*loxP* recombination system for spatiotemporal *HB-EGF* gene ablation. The system generally requires cross-mating of two lines of genetically manipulated mice. One line of mice carries alleles with the *HB-EGF* gene flanked by *loxP* sites [6], and the other line contains a Cre transgene in which the expression of Cre is controlled by *SM22α* or *TIE2* promoter [12,13]. Recombination between the two *loxP* sites in the mated mice results in the catalysis of a deletion of the region flanked by the *loxP* sites (i.e., Cre-dependent transgene expression).

The *SM22α* gene encodes a calponin-related protein that is expressed specifically in adult smooth muscle [14–17]. During mouse embryogenesis, *SM22α* is expressed in cardiac muscle, smooth muscle, and skeletal muscle cells, but becomes restricted to smooth muscle lineages at late embryonic stages and throughout adulthood [18]. The *TIE2* gene encodes an angiopoietin receptor, which is a member of the receptor tyrosine kinase family [19,20]. *TIE2* expression is detected as the first endothelial cells arise, remains positive in endothelial cells throughout development, and is detectable in virtually all endothelial cells of adult tissues [19,21,22].

In this study, we generated smooth muscle and endothelial cell lineage specific HB-EGF knockout mice using Cre/*loxP* system in combination with the *SM22α* and *TIE2* promoter, and demonstrated that HB-EGF in smooth muscle and endothelial lineages was essential for heart development and function.

Materials and methods

Generation of HB-EGF conditional knockout mice using a gene targeting CreloxP strategy. Mice with *HB-EGF* gene flanked by *loxP* sites ($HB^{lox/lox}$) were generated as previously described [6]. Homozygous $HB^{lox/lox}$ mice were bred with *SM22α* or *TIE2* promoter-driven Cre-recombinase transgenic mice [12,13] to generate SM22α-Cre:$HB^{lox/WT}$ or TIE2-Cre:$HB^{lox/WT}$ mice. The obtained mice were bred with $HB^{lox/lox}$ mice to generate SM22α-Cre:$HB^{lox/lox}$ (SM22α-Cre:$HB^{-/-}$) or TIE2-Cre:$HB^{lox/lox}$ (TIE2-Cre:$HB^{-/-}$) mice. The genotype of each mouse was confirmed by PCR. Primers are shown in Table 1.

Table 1
Primer sequences for PCR

Wild-type *HB-EGF* (forward)	5′-CATGATGCTCCAGTGAGTAGGCTCTGATTAC-3′
Wild-type *HB-EGF* (reverse)	5′-AGGGCAAGATCATGTGTCCTGCCTCAAGCC-3′
loxP HB-EGF (forward)	5′-ATGGGATCGGCCATTGAACA-3′
loxP HB-EGF (reverse)	5′-GAAGAACTCGTCAAGAAGGC-3′
Cre recombinase (forward)	5′-TTACCGGTCGATGCAACGAGTGATG-3′
Cre recombinase (reverse)	5′-TTCCATGAGTGAACGAACCTGGTCG-3′
SM22α promoter Cre (forward)	5′-CCAGAGAACAGTGAAGTAGGAG-3′
SM22α promoter Cre (reverse)	5′-CATCCAGTCTTGCGAACCTCAT-3′
TIE2 promoter Cre (forward)	5′-CCCTGTGCTCAGACAGAAATGAGA-3′
TIE2 promoter Cre (reverse)	5′-CGCATAACCAGTGAAACAGCATTGC-3′

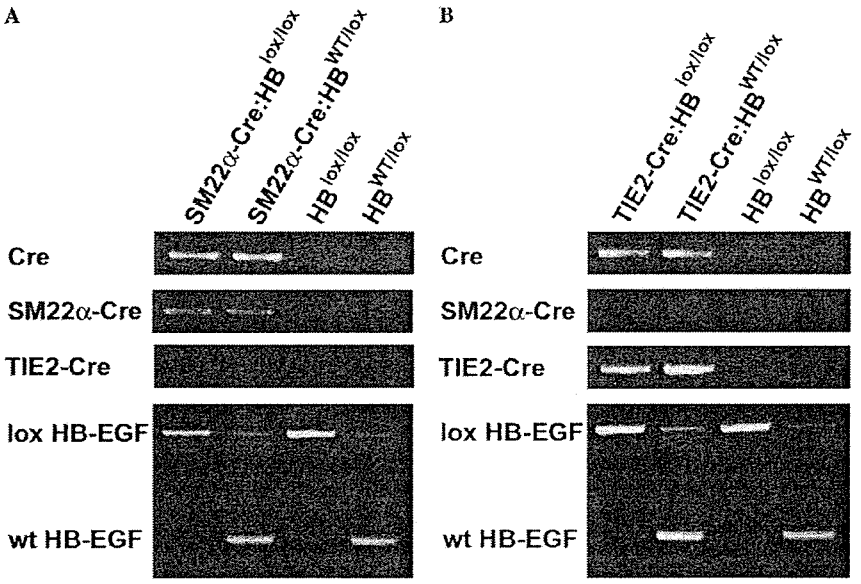

Fig. 1. Genotypes of the conditional knockout mice. SM22α-Cre:$HB^{lox/lox}$ (A) and TIE2-Cre:$HB^{lox/lox}$ (B) mice were confirmed by PCR. *SM22α*-Cre but not *TIE2*-Cre transgenes were detected with SM22α-Cre specific primers and vice versa. The *HB-EGF* gene flanked by *loxP* sites and the wild-type gene were also confirmed by PCR genotyping.

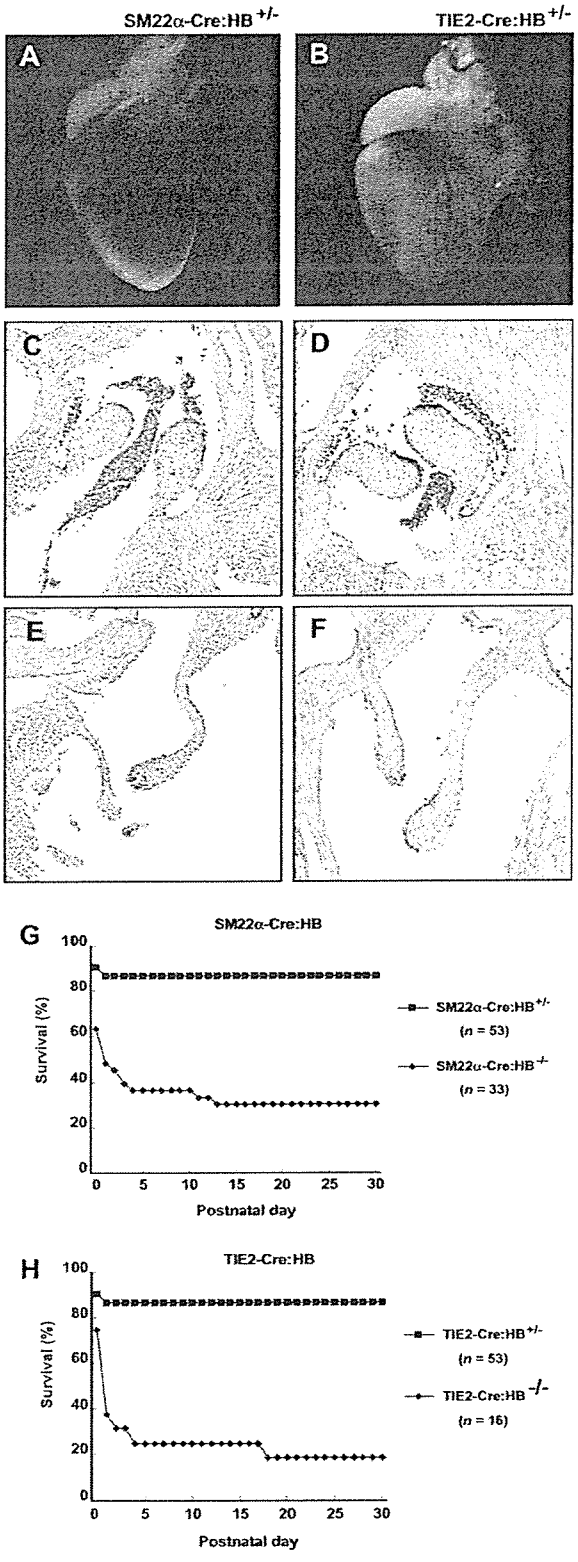

Histological analysis. Mouse tissues were fixed in 3.7% formaldehyde, dehydrated, and embedded in paraffin. Ten micrometer sections were stained with hematoxylin and eosin. For X-gal staining, after fixation with 2% formaldehyde and 0.2% glutaraldehyde, the tissues were stained with 5-bromo-4-chloro-3-indolyl β-D-galactoside (X-Gal). The stained tissues were fixed again with 3.7% formaldehyde, dehydrated, and embedded in paraffin. Ten micrometer sections were stained with eosin.

Results

Generation of HB-EGF conditional knockout mice

To generate cell-type specific HB-EGF knockout mice, mice carrying alleles with the *HB-EGF* gene flanked by *loxP* sites ($HB^{lox/lox}$; [6]) were crossed with SM22α-Cre [12] or TIE2-Cre [13] transgenic mice. The obtained mice carrying the wild-type and *loxP HB-EGF* genes, and Cre transgenes (SM22α-Cre:$HB^{WT/lox}$ or TIE2-Cre:$HB^{WT/lox}$, which we refer to as SM22α-Cre:$HB^{+/-}$ or TIE2-Cre:$HB^{+/-}$) were bred again with $HB^{lox/lox}$ mice to generate SM22α-Cre:$HB^{lox/lox}$ or TIE2-Cre:$HB^{lox/lox}$ mice, which we refer to as SM22α-Cre:$HB^{-/-}$ or TIE2-Cre:$HB^{-/-}$ mice. The genotype of mice was confirmed by PCR analysis (Fig. 1). No overt abnormalities were observed in $HB^{WT/lox}$ or $HB^{lox/lox}$ mice [6,23], and there was no evidence that strong expression of Cre recombinase induced abnormalities in wild-type mice.

HB-EGF expression in the heart of HB-EGF conditional knockout mice

The targeting vector used for the generation of $HB^{lox/lox}$ mice contains the *lacZ* reporter gene under the control of the native *HB-EGF* promoter, which is activated by Cre-mediated recombination [6]. Beta-gal staining of newborn (postnatal day 1; P1) hearts in SM22α-Cre:$HB^{+/-}$ and TIE2-Cre:$HB^{+/-}$ mice showed that HB-EGF was strongly expressed at the site where the great vessels and coronary arteries arise from the heart (Fig. 2A and B). Histological analysis of the heart revealed that β-gal positive cells were localized to the margins of all of the heart valves, including the semilunar (aortic and pulmonic) valves (Fig. 2C and D) and the atrioventricular (mitral and tricuspid) valves (Fig. 2E and F). These results indicate that HB-EGF expression was blocked in the endocardium of the heart valves and the coronary artery of SM22α-Cre:$HB^{-/-}$ and TIE2-Cre:$HB^{-/-}$ mice.

Fig. 2. The heart morphologies and the tissue sections of newborn (P1) SM22α-Cre:$HB^{+/-}$ and TIE2-Cre:$HB^{+/-}$ (corresponds to wild-type) mice and survival of conditional knockout mice. Whole mount β-gal staining revealed that HB-EGF was strongly expressed at sites at which the great vessels and coronary arteries arise from the heart in SM22α-Cre:$HB^{+/-}$ (A) and TIE2-Cre:$HB^{+/-}$ (B) mice. The longitudinal sections showed that HB-EGF was expressed at the margin of the semilunar (C; SM22α-Cre:$HB^{+/-}$ and D; TIE2-Cre:$HB^{+/-}$) and atrioventricular (E; SM22α-Cre:$HB^{+/-}$ and F; TIE2-Cre:$HB^{+/-}$) valves. Over half of the SM22α-Cre:$HB^{-/-}$ (G) and TIE2-Cre:$HB^{-/-}$ (H) mice died within the first day after birth. Approximately 70–80% of these knockout mice died with the first 2 weeks after birth.

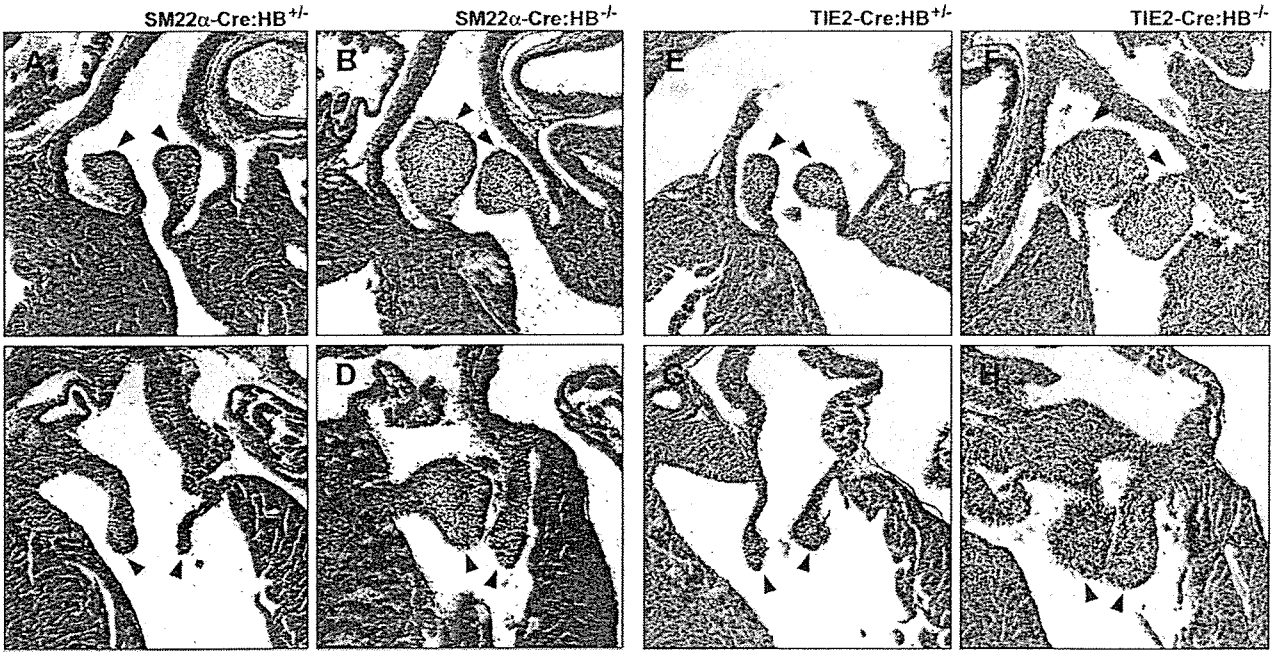

Fig. 3. Hematoxylin and eosin staining of the longitudinal sections of the newborn (P1) heart valves. Histological sections show semilunar (A, B, E and F) and atrioventricular (C, D, G and H) valves. In SM22α-Cre:$HB^{-/-}$ (B and D) and TIE2-Cre:$HB^{-/-}$ (F and H) mice, the valves were enlarged when compared with SM22α-Cre:$HB^{+/-}$ (A and C) and TIE2-Cre:$HB^{+/-}$ (E and G) mice. The valves are indicated with arrowheads.

Postnatal lethality of HB-EGF conditional knockout

Breeding of SM22α-Cre:$HB^{WT/lox}$ or TIE2-Cre:$HB^{WT/lox}$ with homozygous $HB^{lox/lox}$ mice yielded HB-EGF conditional knockout mice. Half of these mice died within one day after birth. Seventy percent of SM22α-Cre:$HB^{-/-}$ mice died within 13 days after birth (Fig. 2G), and 80% of TIE2-Cre:$HB^{-/-}$ mice died within 18 days after birth (Fig. 2H). SM22α-Cre:$HB^{-/-}$ and TIE2-Cre:$HB^{-/-}$ mice survivors displayed no obvious outward abnormalities and remained alive for at least several months after birth (data not shown).

Enlarged heart valves in HB-EGF conditional knockout mice

Histological analysis of newborn (P1) hearts revealed that SM22α-Cre:$HB^{-/-}$ and TIE2-Cre:$HB^{-/-}$ mice developed enlarged semilunar (Fig. 3A, B, E and F) and atrioventricular (Fig. 3C, D, G and H) valves when compared with SM22α-Cre:$HB^{+/-}$ and TIE2-Cre:$HB^{+/-}$ mice. This phenotype was consistent with that of HB-EGF-null mice [6,7]. The enlargement of neonatal heart in HB-EGF-deficient mice [6,7], however, was not observed in the P1 heart of these conditional knockout mice (data not shown).

Cardiac hypertrophy in HB-EGF conditional knockout mice

Although the survivors of SM22α-Cre:$HB^{-/-}$ and TIE2-Cre:$HB^{-/-}$ mice initially appeared normal, massive enlargement of the heart was apparent by 12 weeks of age when compared with control mice (Fig. 4A–D). Specifically, the mean heart-to-body wet weight ratio was $1.64 \pm 0.74\%$ for 12-week-old SM22α-Cre:$HB^{-/-}$ mice and was $0.65 \pm 0.16\%$ for 12-week-old SM22α-Cre:$HB^{+/-}$ mice (Fig. 4E). Further, the mean ratio of heart/body weight was $1.36 \pm 0.48\%$ for 12-week-old TIE2-Cre:$HB^{-/-}$ mice and was $0.76 \pm 0.063\%$ for 12-week-old TIE2-Cre:$HB^{+/-}$ mice (Fig. 4F).

Discussion

The present study demonstrated that loss of HB-EGF in smooth muscle or endothelial cell lineages resulted in heart valve malformations, postnatal lethality, and cardiac hypertrophy, which is a phenotype similar to that of HB-EGF-null mice [6,7]. The *HB-EGF* gene was deleted in endocardial cells of the heart valves in SM22α-Cre:$HB^{-/-}$ and TIE2-Cre:$HB^{-/-}$ mice. Data from the present study suggest that enlargement of the heart valves results from the loss of HB-EGF in the endocardial cells of heart valves, and the heart valve malformation is likely responsible for the postnatal lethality and cardiac hypertrophy of these *HB-EGF* conditional knockout mice.

Heart valves develop from endocardial cushions, which form when the endocardial cells undergo an endocardial-mesenchymal transition (EMT) and proliferate and invade the cardiac jelly, a basement membrane-like substance produced by the myocardial cells. The endocardial cushion area elongates and undergoes continuous remodeling to refine the primitive cushion into thin elongated valve leaflets.

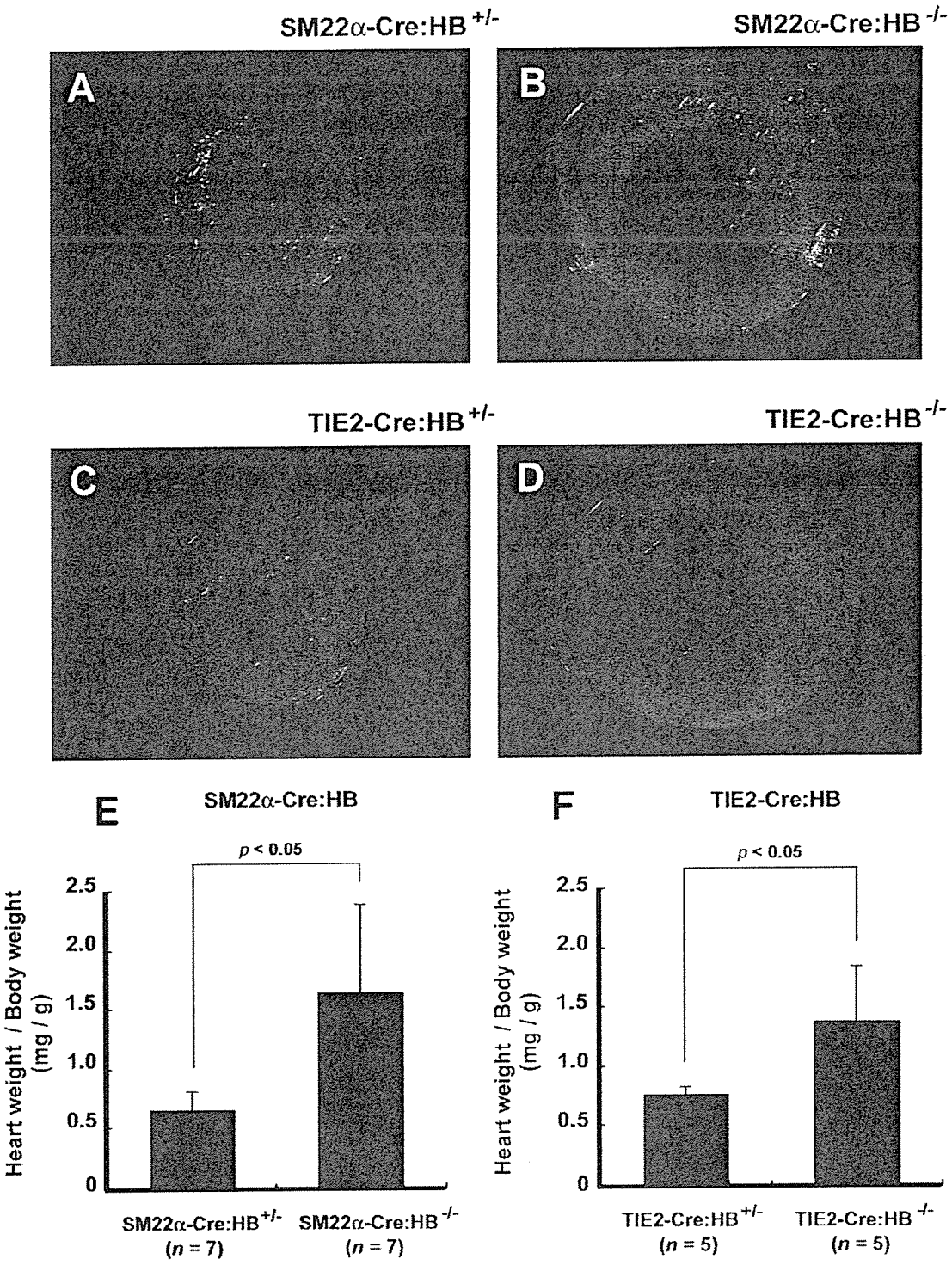

Fig. 4. Cardiac hypertrophy of the conditional knockout mice. Transverse sections of the hearts (A–D) and heart weight-to-body wet weight ratios (E and F) of 12-week-old mice. Values represent means ± SD. Massive enlargement of the heart was observed in SM22α-Cre:HB$^{-/-}$ and TIE2-Cre:HB$^{-/-}$ mice when compared with the control mice.

SM22α is expressed in cardiac muscle, smooth muscle, and skeletal muscle cells during embryogenesis, but becomes restricted to smooth muscle lineages at late embryonic stages and throughout adulthood [18]. Although HB-EGF is expressed in the heart [6,7], we could not detect obvious β-gal staining in myocardium of SM22α-Cre:HB$^{+/-}$ mice. *SM22α-lacZ* mice show the low expression of this transgene in myocardium during late development [24], which

suggests low *SM22α-Cre* activity and subsequent recombination efficiency with *loxP HB-EGF* in myocardium of SM22α-Cre:HB$^{+/-}$ mice. During early avian cardiac development, the endocardium-derived mesenchymal cells, which form endocardial cushions and subsequently form heart valves, have characteristics of smooth muscle-like myofibroblasts and express smooth muscle-specific alpha actin [25]. This finding suggests that the mesenchymal cells that had transformed from endocardial cells expressed the smooth muscle-specific *SM22α* gene, and this fact may account for *HB-EGF* gene deletion in the heart valves of SM22α-Cre:HB$^{-/-}$ mice.

TIE2 is expressed in endothelial cells throughout development [19,21,22]. Previous studies have reported that *TIE2*-Cre:R26R mice have β-galactosidase activity that was restricted to the endocardium and the mesenchyme of the endocardial cushions but was never observed in myocardium or epicardium of the developing heart [26]. These data indicate that the *HB-EGF* gene was eliminated in endocardial but not in myocardial cell lineages in the developing heart of TIE2-Cre:HB$^{-/-}$ mice. Therefore, the present study suggests that the loss of endocardial but not myocardial HB-EGF is at least responsible for the heart valve enlargement in HB-EGF-null mice.

Enlargement of heart valves has also been observed in mutant mice expressing an uncleavable form of proHB-EGF [27], in ADAM17-null mice [7], in EGFR-null mice with a CD1 background, and in mice expressing a mutant EGFR (*waved-2*) [8]. Together with data from the present study, these observations indicate that ectodomain shedding of proHB-EGF in endocardial cells of heart valves and subsequent EGFR activation are essential for remodeling of endocardial cushions. Although the mechanism of cushion remodeling is largely unknown, HB-EGF/EGFR signaling in the mesenchymal cells within the endocardial cushions may suppress cellular proliferation to refine the primitive cushion into thin elongated valve leaflets [7,28]. Recent studies have reported that the cytoplasmic domain of proHB-EGF and C-terminal fragment of proHB-EGF generated by ectodomain shedding have some functions [29–31]. These intracellular signaling might be involved in the heart valve formation.

In conclusion, the loss of *HB-EGF* gene expression in smooth muscle or endothelial cell lineages of the developing mouse results in heart valve malformations and cardiac hypertrophy. These data indicate the significance of endocardial HB-EGF for proper heart development and function.

Acknowledgments

This work is supported by Grants-in-Aid for Scientific Research (No. 17390081) to S.H. from the Ministry of Education, Culture, Sports, Science and Technology of Japan, and Precursory Research for Embryonic Science and Technology (Information and Cell Function).

References

[1] S. Higashiyama, J.A. Abraham, J. Miller, J.C. Fiddes, M. Klagsbrun, A heparin-binding growth factor secreted by macrophage-like cells that is related to EGF, Science 251 (1991) 936–939.
[2] S. Higashiyama, K. Lau, G. Besner, J.A. Abraham, M. Klagsbrun, Structure of heparin-binding EGF-like growth factor: multiple forms, primary structure, and glycosilation of the mature protein, J. Biol. Chem. 267 (1992) 6205–6212.
[3] R. Iwamoto, E. Mekada, Heparin-binding EGF-like growth factor: a juxtacrine growth factor, Cytokine Growth Factor Rev. 11 (2000) 335–344.
[4] E. Nishi, M. Klagsbrun, Heparin-binding epidermal growth factor-like (HB-EGF) is a mediator of multiple physiological and pathological pathways, Growth factors 22 (2004) 253–260.
[5] S. Higashiyama, D. Nanba, ADAM-mediated ectodomain shedding of HB-EGF in receptor cross-talk, Biochim. Biophys. Acta. 1751 (2005) 110–117.
[6] R. Iwamoto, S. Yamazaki, M. Asakura, S. Takashima, H. Hasuwa, K. Miyado, S. Adachi, M. Kitakaze, K. Hashimoto, G. Raab, D. Nanba, S. Higashiyama, M. Hori, M. Klagsbrun, E. Mekada, Heparin-binding EGF-like growth factor and ErbB signaling is essential for heart function, Proc. Natl. Acad. Sci. USA 100 (2003) 3221–3226.
[7] L.F. Jackson, T.H. Qiu, S.W. Sunnarborg, A. Chang, C. Zhang, S. Patterson, D.C. Lee, Defective valvulogenesis in HB-EGF and TACE-null mice is associated with aberrant BMP signaling, EMBO J. 22 (2003) 2704–2716.
[8] B. Chen, R.T. Bronson, L.D. Klaman, T.G. Hampton, J.F. Wang, P.J. Green, T. Magnouson, P.S. Douglas, J.P. Morgan, B.G. Neel, Mice mutant for Egfr and Shp2 have defective cardiac semilunar valvulogenesis, Nat. Genet. 24 (2000) 96–299.
[9] S.W. Sunnarborg, C.L. Hinkle, M. Stevenson, W.E. Russell, C.S. Raska, J.J. Peschon, B.J. Castner, M.J. Gerhart, R.J. Paxton, R.A. Black, D.C. Lee, Tumor necrosis factor-alpha converting enzyme (TACE) regulates epidermal growth factor receptor ligand availability, J. Biol. Chem. 277 (2002) 12838–12845.
[10] U. Sahin, G. Weskamp, K. Kelly, H. Zhou, S. Higashiyama, J. Peschon, D. Hartmann, P. Saftig, C.P. Blobel, Distinct roles for ADAM10 an ADAM17 in ectodomain shedding of six EGFR ligands, J. Cell Biol. 164 (2004) 769–779.
[11] M. Asakura, M. Kitakaze, S. Takashima, Y. Liao, F. Ishikura, T. Yoshinaka, H. Ohmoto, K. Node, K. Yoshino, H. Ishiguro, H. Asanuma, S. Sanada, Y. Matsumura, H. Takeda, S. Beppu, M. Tada, M. Hori, S. Higashiyama, Cardiac hypertrophy is inhibited by antagonism of ADAM12 processing of HB-EGF: metalloproteinase inhibitors as a new therapy, Nature Med. 8 (2002) 35–40.
[12] R. Holtwick, M. Gotthardt, B. Skryabin, M. Steinmetz, R. Potthast, B. Zetsche, R.E. Hammer, J. Herz, M. Kuhn, Smooth muscle-selective deletion of guanylyl cyclase-A prevents the acute but not chronic effects of ANP on blood pressure, Proc. Natl. Acad. Sci. USA 99 (2002) 7142–7147.
[13] P.A. Koni, S.K. Joshi, U.A. Temann, D. Olson, L. Burkly, RA. Flavell, Conditional vascular cell adhesion molecule 1 deletion in mice: impaired lymphocyte migration to bone marrow, J. Exp. Med. 193 (2001) 741–754.
[14] J.P. Lee-Miller, D.H. Heeley, L.B. Smillie, An abundant and novel protein of 22 kDa (SM22) is widely distributed in smooth muscles: purification from bovine aorta, Biochem. J. 244 (1987) 705–709.
[15] S.J. Winder, C. Sutherland, M.P. Walsh, Biochemical and functional characterization of smooth muscle calponin, Adv. Exp. Med. Biol. 304 (1991) 37–51.
[16] J.L. Duband, M. Gimona, M. Scatena, S. Sartore, J.V. Small, Calponin and SM 22 as differentiation markers of smooth muscle: spatiotemporal distribution during avian embryonic development, Differentiation 55 (1993) 1–11.